Magnitude and timing of the antiviral response determine SARS-CoV-2 replication early in infection

Nagarjuna R. Cheemarla[1], Timothy A. Watkins[1,2], Valia T. Mihaylova[1], Bao Wang[1,2], Dejian Zhao[3,4], Guilin Wang[3,4], Marie L. Landry[1,5], and Ellen F. Foxman[1,2*]

[1]Department of Laboratory Medicine, [2]Department of Immunobiology, [3]Department of Genetics, [4]Yale Center for Genomic Analysis, and [5]Department of Internal Medicine, Yale School of Medicine, New Haven CT, U.S.A. 06520

*Corresponding author
Correspondence: ellen.foxman@yale.edu

Abstract

The interferon response is a potent antiviral defense mechanism, but its effectiveness depends on its timing relative to viral replication. Here, we report viral replication and host response kinetics in patients at the start of SARS-CoV-2 infection and explore the impact of these kinetics experimentally. In both longitudinal patient nasopharyngeal samples and airway epithelial organoids, we found that SARS-CoV-2 initially replicated exponentially with a doubling time of ~6hr, and induced interferon stimulated genes (ISGs) with delayed timing relative to viral replication. Prior exposure to rhinovirus increased ISG levels and blocked SARS-CoV-2 replication. Conversely, inhibiting ISG induction abrogated interference by rhinovirus and enhanced SARS-CoV-2 replication rate. These results demonstrate the importance of initial interferon-mediated defenses in determining the extent to which SARS-CoV-2 can replicate at the start of infection and indicate that biological variables that alter the airway interferon response, including heterologous induction of innate immunity by other viruses, could profoundly impact SARS-CoV-2 susceptibility and transmission.

1

Introduction

The novel coronavirus SARS-CoV-2 emerged in late 2019 and has led to a global pandemic, causing over 98M infections and 2.1M deaths at the time of this writing (Dong, 2020). This huge impact has motivated efforts to understand the host immune response to this virus, both to better predict patient outcomes and to design interventions. For an emerging viral infection such as SARS-CoV-2, innate immune responses can be particularly important in host protection, as these responses do not require prior exposure to effectively defend against a pathogen. Studies based on patient samples indicate that dysregulation of innate immune responses late in infection drives immunopathology in severe COVID-19 (Galani et al., 2021; Lee and Shin, 2020; Lucas et al., 2020), but there are relatively few reports describing host responses to SARS-CoV-2 in patients at the start of infection, when innate immune mechanisms are most likely to contribute to host defense.

SARS-CoV-2 enters the body and first replicates in the upper respiratory tract, achieving the highest viral load in the first few days following infection (Wolfel et al., 2020; Zou et al., 2020). High viral load in the nasopharynx correlates strongly with transmissibility in contact tracing studies, and significant viral replication following exposure is likely a prerequisite, although certainly not the only factor, for COVID-19 disease progression (Cevik, 2020; He et al., 2020). A likely candidate for controlling the infection at the earliest stages is the mucosal interferon response. This defense mechanism is initiated when pattern recognition receptors within epithelial cells and immune cells sense general features shared by many viruses, such as common structural features of viral RNA. This recognition event triggers expression of type I and type III interferons (IFNs) and interferon-stimulated genes (ISGs). Secreted interferons, in turn, bind to cell surface receptors on nearby cells, amplifying ISG expression and creating an antiviral state in the mucosal barrier. Many ISGs encode effectors which directly block viral replication within virus target cells, whereas others encode cytokines which recruit and activate cells of the immune system (Odendall and Kagan, 2015; Schneider et al., 2014).

27   Recent evidence supports a protective role for the interferon response in COVID-19, although there is

28   also evidence that the virus antagonizes this response. Recombinant interferon blocks SARS-CoV-2

29   replication in vitro, and genetic deficiencies in the Type I interferon response as well as anti-interferon

30   autoantibodies have been linked to greater COVID-19 disease severity (Bastard et al., 2020;

31   Lokugamage et al., 2020; Pairo-Castineira et al., 2020; Vanderheiden et al., 2020; Zhang et al., 2020).

32   Furthermore, early data from trials of recombinant Type I or Type III interferon for COVID-19 indicate a

33   therapeutic benefit, particularly when patients are treated early in disease(Feld, 2020; Monk, 2020;

34   Wang, 2020).   However, during initial infection of the upper respiratory tract, the kinetics of ISG

35   induction by SARS-CoV-2 are not clear. ISG expression in SARS-CoV-2 infected epithelia can be

36   observed in vitro and in patients, but there is also strong evidence that SARS-CoV-2 antagonizes the

37   interferon response, which likely affects the magnitude and timing of this response (Banerjee et al.,

38   2020; Blanco-Melo et al., 2020; Konno et al., 2020; Martin-Sancho et al., 2020; Ravindra et al., 2020;

39   Xia et al., 2020; Zhou et al., 2020). Since a major beneficial function of ISGs is preventing viral

40   replication, the kinetics of the interferon response early in infection are likely to determine its protective

41   impact, and host and environmental factors which modulate the timing of this response may be key

42   determinants of whether the virus can amplify to a high viral load following infection.

43

44   One factor that can potentially modulate antiviral defenses in the airway epithelium is induction of the

45   ISGs by other viruses, and such effects may be particularly important in limiting viruses which

46   successfully block autologous interferon induction. Rhinovirus, the most frequent cause of the common

47   cold, is frequently detected in the human upper respiratory tract in the presence and absence of

48   symptoms, and both symptomatic and asymptomatic infections can induce ISG expression in the upper

49   respiratory tract mucosa(Landry and Foxman, 2018; Wolsk et al., 2016; Yu et al., 2019). Therefore,

50   rhinovirus is an example of a common environmental factor which could potentially alter the kinetics of

51   ISG expression at the initial target site of SARS-CoV-2 infection, the airway epithelium.

52

53 Here, we studied the initial host response to SARS-CoV-2 infection and its relationship to viral

54 replication, including modulation by rhinovirus infection. Due to SARS-CoV-2 screening and testing

55 practices at our hospital at the start of the pandemic in March 2020, we were able to obtain

56 nasopharyngeal swab samples from patients at different time points post-infection, including serial

57 samples collected close to the start of infection in asymptomatic subjects. Using transcriptomic and

58 biomarker-based analysis of these samples, we observed robust ISG induction in the airway mucosa in

59 response to SARS-CoV-2, but a delay between viral replication and ISG induction. Using an organoid

60 infection model, we modulated the kinetics of ISG induction. We found that enhancing ISG expression

61 by prior exposure to a rhinovirus profoundly inhibited SARS-CoV-2 replication. Blocking ISG induction

62 completely rescued the effects of interference by rhinovirus, and increased replication rate of SARS-

63 CoV-2 in a low MOI infection. These results show the importance of interferon-mediated defenses in

64 restricting SARS-CoV-2 replication at the start of infection and provide an example of how ISG

65 induction by a different virus could impact susceptibility to SARS-CoV-2 infection.

66

67 **Results**

68 **Nasopharyngeal host response to SARS-CoV-2 infection identified by RNA-Seq**

69 The host response to SARS-CoV-2 in the upper respiratory tract and its relationship to viral replication

70 are not well-defined. To characterize host responses during SARS-CoV-2 infection in vivo,

71   we performed RNA-Seq on nasopharyngeal (NP) swab RNA from SARS-CoV-2-positive patients (n=30)

72 and SARS-CoV-2-negative healthcare worker controls (n=8). Patients included outpatients and patients

73 admitted to the hospital of both sexes, who ranged in age from 20s to 90s, with the majority above 60

74 years of age (Fig S1A-D). Samples varied in viral load over >5 orders of magnitude as assessed by RT-

75 qPCR for the SARS-CoV-2 N1 gene or by read mapping of NP RNA to the SARS-CoV-2 genome, with a

76 strong correlation seen between PCR Ct value for the SARS-CoV-2 N1 gene and viral RNA reads by

77 RNA-Seq (r^2=0.8380, p<0.0001; Fig S1E).

78

4

79 Of reads mapping to the human genome, 1770 RNAs differed significantly between SARS-CoV-2+

80 patients and control subjects (Fig 1A). These included 1567 protein-coding genes, of which 1245 (79.4%)

81 were enriched and 322 reduced in patients relative to controls. The most significantly enriched genes in

82 the nasopharynx of SARS-CoV-2 patients were known interferon stimulated genes (ISGs), including three

83 NP ISG transcripts previously shown by our group to accurately identify patients with viral respiratory

84 infection, OASL, IFIT2, and CXCL10 (Fig 1A)(Landry and Foxman, 2018). Analysis of ingenuity pathways

85 and transcription factor binding sites associated with enriched transcripts demonstrated activation of

86 multiple pathways related to ISG induction in SARS-CoV-2 patients compared to controls, as well as

87 other pathways linked to innate immunity, leukocyte recruitment, and initiation of mucosal inflammatory

88 responses (Fig 1B-D).

89

90 Examination of gene expression across patient samples revealed several patterns (Fig 1E-G). First, the

91 45 most significantly enriched genes were all interferon stimulated genes, according to the Interferome

92 database (Rusinova et al., 2013). ISGs appeared to be co-regulated within individual patients, i.e.

93 patients with high expression of one ISG tended to have high expression of other ISGs (Fig 1E). This

94 was also demonstrated by analysis of the correlation between reads for different ISGs across samples

95 (Fig 1F). Second, ISG expression appeared to be loosely correlated with viral load, with those patients

96 with the highest viral load (Fig 1E, left) tending to have higher ISG expression than those with the lowest

97 viral loads (Fig 1E, right). However, while all SARS-CoV-2+ samples showed enrichment of ISG

98 expression compared to controls, direct comparison of DEGs in patient groups with distinct clinical

99 characteristics (sex, age, or outpatient/admitted status) showed no significant differences in ISG

100 expression.

101

102 Next, we measured the level of CXCL10 protein in the NP-swab associated viral transport medium using

103 ELISA. We previously showed that NP CXCL10 is detected in the viral transport medium during other

104 acute viral respiratory infections and correlates with expression of ISGs at the mRNA level (Landry and

105 Foxman, 2018). Consistently, we observed a significant positive correlation between NP CXCL10 protein

106 level with the NP mRNA level of Cxcl10 in SARS-CoV-2+ patient NP samples (Fig 1E, G). Together,

107 these results indicated that across subjects with diverse clinical presentations, SARS-CoV-2 induced a

108 robust interferon response in the nasopharynx and that the NP CXCL10 protein level correlated with ISG

109 expression at the RNA level.

110

111 **Relationship between SARS-CoV-2 viral load and NP host response in vivo**

112 Next, we sought to examine the host response during SARS-CoV-2 infection in a larger set of samples

113 from patients evaluated in our healthcare system in March and April of 2020 (n=140) (Fig 2 and Fig S2A,

114 B), to gain further insight into the relationship between viral replication, disease status, and host response

115 to infection. Based on our previous studies and our finding that NP CXCL10 protein level correlated with

116 ISG expression in SARS-CoV-2 positive samples (Fig 1), we used NP CXCL10 as an indicator of the

117 nasopharyngeal antiviral response. First, we examined NP CXCL10 level in SARS-CoV-2+ individuals

118 who were tested as outpatients and not admitted to the hospital, compared to those who were admitted.

119 Notably, we observed significantly higher NP CXCL10 levels in outpatients compared to admitted patients

120 (Fig 2A, p=0.0019). To understand the reason for this, we first examined patient age, since as a group,

121 admitted patients were significantly older than outpatients (16 years older on average, Fig S2C).

122 However, there was no correlation between age and CXCL10 level (Fig S2D). Next, we examined viral

123 load. We were initially surprised to find that admitted patients had significantly lower viral loads than

124 outpatients (Fig 2B). This suggested that the main factor driving CXCL10 level was viral load. Supporting

125 this idea, correlation analysis showed a significant positive correlation between NP CXCL10 level and

126 viral load by RT-qPCR (for all patients, r^2=0.2030, p<0.0001, Fig 2C). This correlation was also seen in

127 separate analyses of outpatients and admitted patients, with but no significant difference in the slope of

128 the CXCL10 vs viral load correlation between these groups, although there was a trend towards a higher

129 slope in outpatients (Fig 2C). We also observed no significant relationship between sex and NP CXCL10

130 or sex and viral load in this sample set (Fig S2 E,F).

131   Prior work on SARS-CoV-2 has shown that the nasopharyngeal viral load is highest in the first few days

132   of infection, and that the more severe symptoms of COVID-19 requiring hospitalization occur in the

133   second or third week of infection(Cevik, 2020). Therefore, we hypothesized that admitted patients may

134   have shown lower viral loads at the time of testing than outpatients because they presented later in

135   infection, after peak viral replication in the nasopharynx. Consistently, outpatients tended to report fewer

136   days of symptoms prior to testing compared to admitted patients, although this information was only

137   available for a subset of patients (about one-third, n=44; Fig 2D).

138

139   **Viral load and nasopharyngeal CXCL10 patterns in vivo over time**

140   To further evaluate the relationship between viral replication and the innate antiviral response in the

141   nasopharynx, we examined viral load and NP CXCL10 data in longitudinal samples. First, we examined

142   viral load from 29 inpatients from March 12 and April 30, 2020 for whom we had at ≥8 sequential tests

143   results for SARS-CoV-2 with at least the first sample tested using the CDC assay (our clinical laboratory

144   also had other testing platforms) (Fig 3, Table S1). At this time, most serial testing was aimed at patient

145   clearance for discharge. Consistently, the majority of patients (15/29) showed low viral loads (Ct N1>21)

146   which remained low throughout the time course. Another common pattern was high viral load in the first

147   sample (Ct N1<20) followed by a decline in viral load over time, similar to patterns reported in the literature

148   for patients who presented close to the start of symptomatic illness (7/29 patients, Fig 3A). These patients

149   showed high CXCL10 level in the sample with peak viral load and a decline in NP CXCL10 after the viral

150   load had decreased (Fig 3B). One patient had a consistently high NP viral loads for 20 days and did not

151   survive (not shown). Finally, a third pattern was seen in a several patients (6/29), in which the first sample

152   had a low viral load which subsequently increased to a high peak level (Ct N1<20), then decreased over

153   time (Fig 3). This pattern is consistent with patient presentation close to the start of infection. Two of

154   these patients had no symptoms of SARS-CoV-2 and the virus was detected incidentally on screening

155   during hospitalization for other reasons (Fig 3C,D, Table S1). One of these patients had an inconclusive

156   test and a positive test on the same day, 12 hours later (first test, N1 not detected, N2 Ct 38.4, second

7

157   test N1 Ct 34.6, N2 Ct 35.4), suggesting that this might have been the first day of infection for this patient

158   (L2, Fig 3C). The other four patients presented with acute symptoms including fever, and in some cases

159   cough and/or shortness of breath. NP CXCL10 in these patients was undetectable or low in the first

160   positive sample with low viral load, then rose with viral RNA, and then subsequently declined as viral load

161   declined. Together, the longitudinal data show a correlation with NP CXCL10 and viral load in individual

162   patients over time, similar to what we observed across 140 patients tested at a single time point (Fig. 2).

163   Notably, for patient L2, the only patient for whom three samples were available prior to peak viral load,

164   there appeared to be a delay between CXCL10 production relative to viral replication during the first few

165   days of infection, suggesting that initially viral replication outpaced the host innate immune response in

166   the nasopharynx.

167

168   **SARS-CoV-2 replication kinetics and ISG response early in infection**

169   To further evaluate the kinetics of SARS-CoV-2 replication and host response, we performed a time

170   course of SARS-CoV-2 infection using primary human airway epithelial cells grown at air-liquid interface,

171   which differentiate into organoids with beating cilia and mucus production, recapitulating the airway

172   mucosal surface in vivo. Cultures were inoculated with SARS-CoV-2 on the apical surface, washed after

173   1 hr, then incubated at 35°C to simulate the temperature of the upper respiratory tract and conducting

174   airways. Cultures were collected for RNA isolation and RT-qPCR at 1 hr (post-inoculation time point),

175   24hr, 48hr, 72hr, and 96hr and basolateral media was collected for CXCL10 ELISA. Reminiscent of what

176   we observed during SARS-CoV-2 infection in vivo (Fig 3D-I), viral load increased rapidly for the first three

177   days of infection, then plateaued between 72-96 hr (Fig 4A). ISGs were also induced, with ISG mRNA

178   levels and CXCL10 protein level in the basolateral medium increasing markedly from 72 to 96 hr (Fig 4B-

179   F). Notably, a very high level of CXCL10 protein was produced by infected epithelia (~4ng/ml by 96 hr),

180   consistent with the strong NP CXCL10 signal observed in the nasopharynx in vivo.

181

182

Doubling time of SARS-CoV-2 in vitro and in vivo

Viral replication in organoid cultures appeared to follow an exponential curve for the first 72hr of infection. Therefore, we used curve-fitting to exponential growth to estimate the doubling time, which was 5.858 hr (95% C.I. of 4.85-7.357 hr., based on 20 y-values, 5 per time point; Fig 4G). For patient L2, viral load data from first three SARS-CoV-2+ time points also appeared to follow exponential growth, therefore we used the same method to estimate the SARS-CoV-2 doubling time in vivo from this data, which was 6.454 hr (95% C.I. 4.261-13.30 hr based on 3 y-values, Fig 4H). For all other patients from whom viral load increased in serial samples (Fig 3), we had only one sample prior to peak viral load. We asked what the doubling times for SARS-CoV-2 would be in these samples if we assumed exponential replication between the first and peak viral RNA values. The calculated doubling times across patients ranged from 3.048-6.509 hr for samples less than or equal to 5 days apart. For the two patients with a larger sampling interval (L44, L12), calculated doubling times were 9.455 and 12.58 hr, although these calculations would be expected to overestimate doubling time if the second sample was taken after viral replication had plateaued or begun to decline. Together, the in vitro and in vivo results indicate that SARS-CoV-2 replicates exponentially during the first few days post-infection prior to the peak host anti-viral response, with an average doubling time of approximately 6 hr.

Effect of prior rhinovirus infection on ISG induction and SARS-CoV-2 replication

One of the many physiological exposures that could potentially alter the local innate immune response to SARS-CoV-2 in the upper airway mucosa is recent infection by other viruses. To model this situation, we used organoid culture to examine the effects of prior exposure to rhinovirus, the most frequently detected virus in the human upper respiratory tract, on subsequent SARS-CoV-2 infection (Fig 5A). Based on previous studies, we expected that rhinovirus might curtail infection by inducing an epithelial antiviral response, but also could potentially promote infection by increasing expression of SARS-CoV-2 entry receptors (Wu et al., 2020; Ziegler et al., 2020). Similar to previous observations, rhinovirus infection (HRV-01A, MOI ~0.05) led to robust induction of interferon stimulated genes by day 3 post-infection (Fig

9

209   5B). We then evaluated whether rhinovirus infection altered the expression of ACE2, the SARS-CoV-2

210   entry receptor. ACE2 was originally reported to be an ISG, but a subsequent study reported that full-

211   length ACE2, which functions as an entry receptor, is not an ISG, and that a truncated form, dACE2, is

212   an ISG but is not a functional SARS-CoV-2 entry receptor (Onabajo et al., 2020; Ziegler et al., 2020).

213   Consistent with this finding, we observed that dACE-2 was significantly induced by rhinovirus infection

214   (~14-fold) and that, as expected for an ISG, induction was prevented by blocking activation of IRF3, a

215   transcription factor downstream of viral RNA sensors, using the inhibitor BX795 (Clark et al., 2009). In

216   contrast, full-length ACE2 expression was slightly but significantly increased by rhinovirus infection(~2-

217   fold) and this change was not abrogated by BX795, suggesting a different mechanism of induction (Fig

218   S3.) Rhinovirus infection had no effect on expression of TMPRSS2 (not shown).

219

220   Next, we evaluated SARS-CoV-2 replication and ISG induction following infection of airway epithelial

221   organoids, with or without prior rhinovirus infection. SARS-CoV-2 viral load increased exponentially in

222   infected cultures without prior RV infection, as observed previously (Fig 4), but showed essentially no

223   increase when cultures had been exposed to rhinovirus 3 days prior (Fig 5C). Evaluation of ISG

224   expression over the course of infection showed that at early time points of SARS-CoV-2 infection (24, 48

225   hr, and sometimes 72hr), ISGs were significantly more highly expressed in RV-preinfected cultures that

226   in cultures infected with SARS-CoV-2 without prior RV exposure (Fig 5D). This included several ISGs

227   which have been previously reported to limit coronavirus replication or for which polymorphisms are

228   linked to disease severity of SARS-CoV or SARS-CoV-2, including ISG15, BST2 (tetherin), and LY6E,

229   and OAS1-3 (Hamano et al., 2005; He et al., 2006; Ma et al., 2014; Martin-Sancho et al., 2020; Pairo-

230   Castineira et al., 2020; Pfaender et al., 2020; Taylor et al., 2015) (Fig 5D). Non-linear regression analysis

231   was consistent with exponential replication of SARS-CoV-2 from 24-72 hr post infection in mock-

232   pretreated cultures, in contrast to rhinovirus pre-infected cultures which supported essentially no

233   replication (Fig 5E).

234

235   To better understand the timing and breadth of the epithelial host response to rhinovirus that appeared

236   to limit SARS-CoV-2 replication, we evaluated ISG expression over time for five days post rhinovirus

237   infection and examined ISG expression and viral infection at the single cell level. Time course analysis

238   showed that following inoculation, rhinovirus replicated robustly, peaking at 24 hr post-infection, and then

239   declined significantly but was still detectable by RT-qPCR at day 5, a time point corresponding to 48 hr

240   post SARS-CoV-2 infection in the sequential infection experiment (FigS4A). ISG expression increased

241   and decreased in parallel with viral replication but was still significantly higher than in mock-treated cells

242   at day 5 post-rhinovirus infection(Fig S4B-E). Next, we performed single cell RNA sequencing to evaluate

243   the host ISG response in infected and bystander cells on day 5 post rhinovirus infection. At this time

244   point, rhinovirus viral RNA reads were detected in only 70 out of 4200 cells sequenced (Fig 5F). The

245   infected cells were predominantly ciliated cells but included all major cell types, consistent with the HRV-

246   01A entry receptor LDL-R being ubiquitously highly expressed throughout the culture (Fig S4F,G).

247   Although rhinovirus was only detected in a small subset of cells in infected cultures at day 5 (1.67%),

248   ISGs were elevated in all cells compared to mock-treated cultures (Fig 5F), demonstrating that rhinovirus

249   infection induces a robust bystander antiviral response in uninfected cells that lasts at least 5 days.

250

251   **Blocking ISG induction restores SARS-CoV-2 replication following rhinovirus infection**

252   Next, to test whether suppression of SARS-CoV-2 replication by rhinovirus was dependent upon the host

253   cell interferon response, we pre-treated cells with the signaling inhibitor BX795 18hr before rhinovirus

254   infection, which prevents interferon and ISG induction by rhinovirus(Fig 6A, B)(Clark et al., 2009; Wu et

255   al., 2020). There was no significant difference in SARS-CoV-2 viral load in RNA isolated from organoid

256   cultures at 72 hr for cultures with and without drug treatment, (Fig 6B). The effect of BX795 treatment

257   was much more striking in the setting of sequential rhinovirus-SARS-CoV-2 infection. As seen previously

258   (Fig 5), prior infection with rhinovirus suppressed SARS-CoV-2 replication by >1000-fold, but replication

259   was restored by BX795 pre-treatment (Fig 6C). These results indicate that IRF3 signaling is critical for

11

260 the inhibition of SARS-CoV-2 replication by prior rhinovirus infection, consistent with the effects of RV

261 pre-infection on ISG induction (Fig 5).

262

263 RV viral RNA was detected at much lower levels than SARS-CoV2 RNA at this time point (72hr post

264 SARS-CoV-2 infection, 6 days post-RV infection), and showed a slight reduction during SARS-CoV-2

265 coinfection without BX-795, but significantly higher levels during co-infection in the presence of BX-795.

266 This result indicates that the antiviral response limits rhinovirus replication in the setting of SARS-CoV-2

267 co-infection at this time point, and that both viruses achieve higher viral loads with inhibition of innate

268 antiviral signaling. In other words, in the presence of an intact antiviral response, viral load of both viruses

269 is reduced by co-infection, but if the host response is inhibited, the viral load of both viruses is higher

270 during co-infection. This experiment models viral co-infection in a host with an intact interferon response

271 (both viruses decrease during co-infection), compared to a host with a deficient interferon response

272 (equal or greater replication of both viruses during co-infection.)

273

274 **Blocking ISG induction enhances SARS-CoV-2 replication in a low MOI infection**

275 Next, we further probed the effect of BX-795 treatment on SARS-CoV-2 replication using a ten-fold lower

276 MOI (MOI ~0.05), conditions under which SARS-CoV-2 would potentially be more sensitive to

277 suppression by ISGs. Under these conditions, BX795 treatment led to a ~10-fold increase in intracellular

278 viral load and ~300-fold increase in virus shedding into the apical wash at 72 hr post infection. A trend

279 towards an increase (5-10x) was also seen at 96 hrs post-infection, although due to variability among

280 replicates this difference was not statistically significant (Fig 7A, B). Based on these results, we checked

281 the effect of BX795 on viral shedding into the apical wash in the MOI 0.5 infection (Fig 6) but in this case

282 results were similar to those observed in organoid cultures (not shown). Next, based on the increase in

283 viral RNA from 1hr to 72 hr during the low MOI infection, we estimated the effect of BX795 on the SARS-

284 CoV-2 doubling time in organoid culture. Assuming exponential growth between 1hr and 72 hr, the SARS-

285 CoV-2 doubling time without BX795 was 5.127 hr (95%C.I. 3.889 to 7.518 hrs), and with BX795 was

12

286   3.578 hr (95%C.I. 3.499 to 3.661). We then examined expression of ISGs that have been shown to limit

287   coronavirus replication and which have high basal expression in airway epithelial cultures including

288   IFITM3, ISG15, and BST2 (tetherin), thus could be particularly important for limiting a low MOI infection.

289   Induction of all of these ISGs was suppressed by BX795 pre-treatment (Fig 7D-F). For BST2 mRNA,

290   blocking ISG induction with BX795 revealed a decrease in BST2 mRNA below the baseline level during

291   SARS-CoV-2 infection, suggesting that SARS-CoV-2 may antagonize BST2 expression at the mRNA

292   level, in addition to other mechanisms whereby SARS-CoV-2 or SARS-CoV have been reported to

293   antagonize BST2 at the protein level (Martin-Sancho et al., 2020; Taylor et al., 2015). The effects of

294   BX795 on SARS-CoV-2 during low MOI infection indicate that the epithelial antiviral response induced

295   by SARS-CoV-2 does limit viral replication, albeit to a lesser extent than interference by rhinovirus.

296

297   Taken together, our results show that SARS-CoV-2 undergoes exponential replication at the start of

298   infection and induces ISG expression in vitro and in vivo, and that conditions which alter the initial ISG

299   expression level or rate of ISG induction, including prior infection by a different virus, can profoundly

300   impact SARS-CoV-2 replication.

301 **Discussion**

302 SARS-CoV-2 replication in the nasopharynx is known to peak during the first week of infection, but the

303 biological variables governing the rate and magnitude of viral amplification are not fully understood

304 (Cevik, 2020; He et al., 2020). Nasopharyngeal viral load early in infection correlates with likelihood of

305 transmitting the infection, and robust viral amplification in the respiratory tract is also likely a prerequisite,

306 although certainly not the only factor, for progression of COVID-19 disease. Here we present evidence

307 that during the first few days of SARS-CoV-2 infection, the airway interferon response plays a protective

308 role by curtailing viral replication in its initial target tissue: the airway epithelium. Specifically, our data

309 show that the extent of viral replication is determined by the magnitude and timing of the host interferon

310 response during a critical time window at the start of infection.

311

312 The interferon response is a potent mechanism of antiviral innate defense at mucosal surfaces and

313 effectively curtails replication of many viruses, most of which also antagonize this host response to some

314 degree in order to enable viral replication(Garcia-Sastre, 2017; Iwasaki, 2012). Viral recognition by innate

315 immune sensors within infected epithelial cells induces expression of type I and type III interferons and

316 interferon stimulated genes (ISGs), a diverse family of antiviral effectors, both directly, in infected cells,

317 and in neighboring cells through paracrine effects of secreted interferons(Odendall and Kagan, 2015;

318 Schneider et al., 2014). SARS-CoV-2 has been reported to induce interferons and ISGs in the airway

319 mucosa in vivo and in vitro (Mick et al., 2020; Mulay et al., 2020; Ravindra et al., 2020; Zhou et al., 2020).

320 Consistently, we observed robust ISG induction in all patients using RNA-Seq of nasopharyngeal RNA,

321 regardless of disease severity or other biological variables (Fig 1). However, there is also convincing

322 evidence that SARS-CoV-2 antagonizes the interferon response in infected cells through multiple

323 mechanisms(Banerjee et al., 2020; Konno et al., 2020; Martin-Sancho et al., 2020; Xia et al., 2020). Our

324 observations with organoid culture (Fig 4), and in the one patient for whom we had multiple longitudinal

325 samples prior to peak viral load (patient L2, Fig 3A) show exponential viral replication at the start of

326 SARS-CoV-2 infection. ISGs are also induced, but it is unclear when this host response becomes

14

327   functionally effective. We found that in the first 72 hours of infection, prior to the peak host response,

328   blocking ISG induction had no effect in SARS-CoV infection at MOI 0.5 (Fig 6), but did increase viral

329   replication at ten-fold lower MOI (Fig 7; MOI 0.05). Together, these observations support a model in which

330   antagonism by SARS-CoV-2 attenuates but does not prevent the interferon response and thereby creates

331   a time window at the start of infection during which the virus can undergo exponential growth.

332

333   Due to the nature of exponential growth, a small change in biological variables affecting either the rate of

334   viral replication or the rate of development of an effective interferon response could have a profound

335   impact on viral amplification and peak viral load. For example, based on an average viral doubling time

336   estimated from our data of ~6 hr, a 24 hour delay in the development of an effective interferon response,

337   for example due to host deficiency in innate immune signaling, would lead to a 16-fold increase in peak

338   viral load. Thus, a peak viral load of 1000 infectious particles would become 16,000 infectious particles,

339   an upper airway viral load much more likely to lead to viral transmission or spread of the infection to the

340   lower respiratory tract. Likewise, if conditions or viral differences allowed the viral doubling time to

341   decrease by two hrs, from 6 hr to 4hr, this would lead to 16-fold greater viral amplification by 48 hr, and

342   64-fold greater amplification by 72hr, for the faster growing strain. The extent to which NP viral load

343   correlates with disease severity is still unclear, although several studies show an association (Huang et

344   al., 2020; Liu et al., 2020; Yilmaz et al., 2020; Zheng et al., 2020). However, there is strong evidence that

345   high NP viral load correlates with viral transmission, an issue that has come into focus recently due to

346   the emergence of SARS-CoV-2 strains that appear to have enhanced transmission, such as the B.1.1.7

347   strain emerging in the U.K.(Cevik, 2020; He et al., 2020; Prevention, 2021; Singanayagam et al., 2020)

348   Our study predicts biological features of the virus that could potentially underlie this greater

349   transmissibility, such as better antagonism of the host interferon response or faster doubling time, both

350   of which would be expected to increase NP viral load and therefore increase transmissibility.

351

352 Conversely, host factors that enhance interferon-mediated defenses could be impactful in reducing peak

353 viral load or even preventing infection altogether. One factor that is known to alter ISG expression in the

354 nasopharynx is recent viral infection. In this study, we focused on rhinovirus, the most frequent cause of

355 the common cold. Recent epidemiological studies have shown that this virus is much more prevalent in

356 the upper respiratory tract than previously appreciated (Foxman and Iwasaki, 2011; Jartti et al., 2008).

357 For example, in a recent year-round study, about one-third (34%) of all nasal samples from young children

358 (<5 yrs) were rhinovirus-positive, regardless of symptoms (Byington et al., 2015). Rhinoviruses and other

359 respiratory viruses have also been shown to induce ISGs in the nasopharynx in vivo, in both the presence

360 and absence of symptoms (Landry and Foxman, 2018; Wolsk et al., 2016; Yahya et al., 2017; Yu et al.,

361 2019). Thus, rhinovirus fits the characteristics of a common environmental factor that could impact ISG

362 expression in the respiratory tract.

363

364 Our data using sequential infection in an airway epithelial organoid model show that prior rhinovirus

365 infection blocks replication of SARS-CoV-2 that this protection is dependent upon ISG induction.

366 Furthermore, using time course studies and single cell analysis of organoid cultures, we found that a

367 significant bystander interferon response can be detected in cells throughout the epithelium for at least 5

368 days post-rhinovirus infection, even though viral replication peaks at 24 hr and few infected cells are

369 detected at this time point (Fig 5, Fig S4). This finding is consistent with recent work from our group and

370 others showing that the host interferon response triggered by one respiratory virus can block infection by

371 another (Essaidi-Laziosi et al., 2020; Wu et al., 2020). Viral interference seen during sequential influenza

372 virus infections was in fact the basis for the original discovery and naming of interferons in 1957, but only

373 recently has this idea been explored in depth with regards to human respiratory viral infections, triggered

374 in part by epidemiological data suggesting interference among RNA respiratory viruses(Greer et al.,

375 2009; Isaacs and Lindenmann, 1957; Karppinen et al., 2016; Nickbakhsh et al., 2019; Schultz-Cherry,

376 2015). ISG induction by an unrelated virus may be particularly effective against a virus like SARS-CoV-

377 2, since it would pre-empt many of the mechanisms SARS-CoV-2 has in place to antagonize interferon

16

378 and ISG induction in response to its own replication, including specific targeting of ISGs effective in

379 blocking the coronavirus life cycle such as BST2 (Martin-Sancho et al., 2020; Taylor et al., 2015).

380

381 The concept of viral interference based on the host interferon response assumes a host with intact innate

382 immune defenses, which may not always be the case. In our experimental model, there was a profound

383 difference in the outcome of rhinovirus-SARS-CoV-2 co-infection in the presence and absence of an

384 intact host cell interferon response (Fig 6). With an intact host response, viral loads of both viruses

385 decreased, but when the interferon response was blocked, viral loads of both viruses were equal to or

386 higher than in single infections (Fig 6.) This result illustrates that the expected outcome of a viral co-

387 infection is not one-size-fits-all: it is likely to be profoundly dependent upon host innate immune status.

388 Many host factors ranging from genetic polymorphisms to transient environmental conditions in the

389 airway (e.g. temperature, humidity) can attenuate interferon responses and promote replication of

390 respiratory viruses, and would likewise be expected to reduce the interferon-mediated protective effects

391 of viral co-infection (Asgari et al., 2017; Foxman et al., 2015; Kudo et al., 2019; Lamborn et al., 2017;

392 Mihaylova et al., 2018; Zhang et al., 2020). Also, interference requires closely spaced virus co-exposures,

393 which may be less frequent at certain times of the year, or during the use of pandemic mitigation

394 measures. Low rates of influenza during 2020 in the southern hemisphere indicate that the public health

395 measures put in place to slow the spread of SARS-CoV-2 also suppressed circulation of other respiratory

396 viruses, although there is some evidence that rhinoviruses have continued to circulate(Olsen et al., 2020;

397 Poole et al., 2020). Viral interference may become a more important consideration for understanding

398 susceptibly to COVID-19 and other viral pathogens as society reopens.

399

400 There are several important caveats to our study. First, our data indicate a relatively limited effect of the

401 SARS-CoV-2-induced interferon response on initial viral replication when it is the only virus present, at

402 least at high MOI (Fig 6). However, the recruitment of cells of the immune system to the respiratory tract,

403 as indicated by our RNAseq data (Fig 1), could considerably amplify ISG induction in vivo. Recent work

17

404   showing that interferon deficiencies are linked to severe COVID-19 indicates the importance of interferon-

405   mediated defense against this virus in vivo (Bastard et al., 2020; Pairo-Castineira et al., 2020; Zhang et

406   al., 2020). Second, in vivo virus-host-virus interactions could be more complicated than those seen in

407   organoid culture; for example, if a viral infection results in residual lung damage this could exacerbate

408   rather than protect against a subsequent viral respiratory illness. Studying virus-host-virus interactions in

409   vivo will be an important future direction of this study. For assessing viral interference, it will be critical

410   not only to look at co-occurrence or sequential occurrence of viral infections, but also to measure the

411   antiviral response in vivo. For example, symptomatic upper respiratory tract infections induce greater

412   ISG responses than asymptomatic, and the latter may not cause significant interference(Yahya et al.,

413   2017). Such studies will be facilitated by increasing development of nasopharyngeal swab-based

414   methods to assess the airway host immune response, as presented here and in the recent

415   literature(Landry and Foxman, 2018; Mick et al., 2020; Wolsk et al., 2016; Yu et al., 2019).

416

417   In sum, our results demonstrate an important role for the interferon-mediated defenses in curtailing

418   SARS-CoV-2 replication at the start of infection and compel further studies of how the changing

419   conditions present in the upper respiratory tract, including recent infection by other viruses, can modulate

420   host antiviral defenses and alter SARS-CoV-2 infection and transmission.

430

Author Contributions

432   Conceptualization E.F.F.; Methodology, N.R.C., T.W., V.T.M., B.W., D.Z., M.L.L., and E.F.F.;

433   Investigation N.R.C., T.W., V.T.M., B.W., and E.F.F.; Formal analysis B.W., D.Z., and G.W.; Resources,

434   M.L.L.; Writing – Original Draft, E.F.F.; Writing – Review & Editing, N.R.C., T.W., V.T.M., B.W.,D.Z., G.W.,

435   M.L.L., E.F.F.; Funding Acquisition, E.F.F.

436

Declaration of Interests

438   Dr. Foxman is an inventor on a pending patent application WO2019/217296 A1 and Dr. Foxman and Dr.

439   Landry are inventors on pending patent application WO2018/071498 Al. The other authors declare no

440   competing interests.

441 **Methods details**

442 **RESOURCE AVAILABILITY**

443 **Lead Contact**

444 Further information and requests may be directed to, and will be fulfilled by the lead

445 contact Ellen F. Foxman, ellen.foxman@yale.edu

446

447 **Materials availability**

448 This study did not generate new reagents.

449

450 **Data and Code Availability**

451 Nasopharyngeal transcriptome data and single cell RNA sequencing data will be publicly available in the

452 GEO database at the time of publication.

453

454 **EXPERIMENTAL MODEL AND SUBJECT DETAILS**

455 *Ethics statement*

456 The use of clinical samples and data in this study was approved by the Yale Human Research Protection

457 Program Institutional Review Board (Protocol ID #200002765). Procedures for testing residual clinical

458 samples and recording linked patient data, followed by sample and data de-identification, were evaluated

459 and the requirement for specific patient consent was waived. In vitro experiments used primary human

460 cells obtained from Lonza Bioscience (Walkersville, Maryland, U.S.A.). Lonza guarantees that all tissue

461 utilized for human cell products is ethically obtained with donor informed consent in accordance with

462 processes approved by an Institutional Review Board or comparable independent review body.

463

464 *Clinical samples*

465 We used viral residual nasopharyngeal (NP) samples remaining after clinical testing for CXCL10

466 measurements and transcriptome analysis. Swab-associated viral transport medium was stored at -80

467   °C following clinical testing and thawed just prior to ELISA assay or RNA isolation for RNA-Seq. Clinical

468   information including age, sex, virology results, and specific features of clinical course including

469   presenting symptoms, hospital admission and length of stay, was extracted from the electronic medical

470   record and recorded, after which samples were assigned a study code and de-identified. In the clinical

471   laboratory, SARS-CoV-2 was detected in most samples using an EUA-approved TaqMan assay detecting

472   the CDC targets N1, N2, and RNAseP (Prevention, 2020). In some longitudinal samples, SARS-CoV-2

473   was diagnosed with the commercial Cepheid assay (reference); in this case, RT-qPCR for the CDC N1

474   gene was repeated using RT-qPCR TaqMan assay for the CDC N1 gene as described previously (Cat

475   no: 10006600, Integrated DNA Technologies, IA)(Vogels et al., 2020).

476

477   *Primary human bronchial epithelial cells.*

478   Primary human bronchial epithelial cells from healthy adult donors were obtained commercially (Lonza,

479   Walkersville, MD, USA) and cultured at air-liquid interface according to manufacturer's instructions using

480   reduced hydrocortisone (Stem Cell Technologies, Vancouver, Canada). Cells were allowed to

481   differentiate for four weeks by which time they displayed beating cilia and mucus production.

482

483   *Viruses*

484   Rhinovirus 1A (HRV-01A; ATCC VR-481) was amplified in H1-HeLa cells (ATCC CRL-1985) and titer

485   was determined by plaque assay as reported previously (Foxman et al., 2015). SARS-CoV-2 (BEI

486   resources, USA-WA1/2020) was generously provided by the Wilen lab. Virus was cultured on Vero E6

487   cells and titer was determined by plaque assay as described previously (Ravindra et al., 2020).

488

489   *RNA isolation from clinical samples*

490   At the time of accessioning, the residual viral transport medium from clinical samples was stored at -80C.

491   Upon thawing, RNA was isolated from 140μl of transport medium using the Qiagen Viral RNA isolation

492   kit per manufacturer's instructions (Ref: 52904, Qiagen, Germany) and one aliquot was reserved for

493   ELISA.

494   *Library preparation and RNA Sequencing*

495   RNA samples were quantified and checked for quality using the Agilent 2100 Bioanalyzer Pico RNA

496   Assay. Library preparation was performed using Kapa Biosystem's KAPA HyperPrep Kit with RiboErase

497   (HMR) in which samples were normalized with a total RNA input of 25ng. Libraries were amplified using

498   15 PCR cycles. Libraries were validated using Agilent TapeStation 4200 D1000 assay and quantified

499   using the KAPA Library Quantification Kit for Illumina® Platforms kit. Libraries were diluted to 1.3nM and

500   pooled at 1.25% each of an Illumina NovaSeq 6000 S4 flowcell using the XP workflow to generate 25M

501   read pairs / sample.

502

503   *RNA-Seq data analysis*

504   Low quality reads were trimmed and adaptor contamination was removed using Trim Galore (v0.5.0,

505   https://www.bioinformatics.babraham.ac.uk/projects/trim_galore/). Trimmed reads were mapped to the

506   human reference genome (hg38) using HISAT2 (v2.1.0)(Kim et al., 2019). Gene expression levels were

507   quantified using StringTie (v1.3.3b) with gene models (v27) from the GENCODE project(Pertea et al.,

508   2015). Differentially expressed genes (adjusted p value < 0.05, fold change cutoff = 2) were identified

509   using DESeq2 (v 1.22.1) (Love et al., 2014). To avoid the unexpected outlier replacement for sex-linked

510   genes, we turned off the outlier replacement option in the male vs. female comparison by setting

511   minReplicatesForReplace=Inf for the DESeq() function in the DESeq2 package.

512

513   *Visualization of RNA-Seq data.* Protein coding genes differentially expressed in SARS-CoV-2+ vs.

514   negative control were visualized on a volcano plot, with an x-axis cutoff | $\log_2$FC cutoff | =10. All

515   differentially expressed RNAs are included in Table S1 (n=1770). Significantly differentially expressed

516   transcripts were defined as those with $\log_2$FC>1 and adjusted p value<0.05. Heatmap shows gene

517   expression levels of top 45 most significant DEGs using min-to-max scaling of normalized read counts.

22

518   Pathway analysis was performed using Ingenuity Pathway Analysis (version 01-16). Transcription factor

519   motif enrichment analysis was performed using Cytoscape (version 3.8.1) with the iRegulon plug-in

520   ((version 1.3)(Janky et al., 2014).

521

522   *In vitro infections*

523   We infected primary human bronchial epithelial cells differentiated at air-liquid interface with HRV-01A,

524   SARS-CoV-2, or both. For SARS-CoV-2, high MOI infection was MOI 0.5 and low MOI infection was MOI

525   0.05. For HRV-01A, MOI 0.1 was used, as this was the minimum viral inoculum that reproducibly led to

526   robust HRV-01A viral replication in ALI cultures based on prior studies.

527

528   To evaluate the effect of RV on subsequent infection with SARS-CoV-2, we infected with each virus

529   individually or sequentially and examined the time course of viral amplification and ISG induction. To

530   formally test whether prior exposure to RV inhibits SARS-CoV-2 replication through activation of the host

531   cell interferon response, we performed sequential infection studies in the presence of BX795.

532

533   *RT-qPCR*

534   For RT-qPCR, RNA was isolated from each well of differentiated epithelial cells using the QIAGEN

535   RNeasy kit by incubating each 24-well insert with 350 μl lysis buffer at room temperature for 5 minutes,

536   followed by RNA isolation and cDNA synthesis using iScript cDNA synthesis kit (BioRad). To quantify

537   viral RNA and mRNA levels for interferon stimulated genes and the housekeeping gene HPRT, qPCR

538   was performed using SYBR green iTaq universal (BioRad) per manufacturer's instructions. Viral RNA

539   was quantified using primers to the RV genome. Viral RNA per ng total RNA is graphed as fold change

540   from the limit of detection (40 cycles of PCR) as 2^{40-Ct}. ISG mRNA levels are graphed as fold change from

541   mock-treated cells or are presented relative to the level of mRNA for the housekeeping gene HRPT (2^{-}

542    $^{\Delta\Delta CT}$). RT-qPCR for SARS-CoV-2 within cultures was performed using the previously-described TaqMan

543   assay for the CDC N1 gene with primers and probes provided by IDT (Cat no: 10006600, Integrated DNA

544   Technologies, IA). RT-qPCR for SARS-CoV-2 in apical was performed using a combined reverse

545   transcriptase and qPCR reaction using the Luna Universal Probe One-Step RT-qPCR Kit (New England

546   Biolabs, MA)

547

548   The following primers were used for RT-qPCR with SYBR green:

549   HPRT (F-TGGTCAGGCAGTATAATCCAAAG; R- TTTCAAATCCAACAAAGTCTGGC)

550   ISG15 (F-CATCTTTGCCAGTACAGGAGC; R-GGGACACCTGGAATTCGTTG)

551   RSAD2 (F-TCGCTATCTCCTGTGACAGC;R-CACCACCTCCTCAGCTTTTG)

552   MX1 (F-AGAGAAGGTGAGAAGCTGATCC;R-TTCTTCCAGCTCCTTCTCTCTG)

553   IFITM3 (F-ATCGTCATCCCAGTGCTGAT;R-ATGGAAGTTGGAGTACGTGG)

554   IFIT2 (F-CCTCAAAGGGCAAAACGAGG; R-CTGATTTCTGCCTGGTCAGC)

555   CXCL10 (F-CCTGCAAGCCAATTTTGTCC; R-ATGGCCTTCGATTCTGGATTC

556   LY6E (F-GCATTGGGAATCTCGTGACA; R-ATGGAAGCCACACCAACATT)

557   BST2 (F-CACACTGTGATGGCCCTAAT; R-TGTAGTGATCTCTCCCTCAAGC)

558   IFITM3 (F-ATCGTCATCCCAGTGCTGAT; R-ATGGAAGTTGGAGTACGTGG)

559   OAS1 (F-GCTCCTACCCTGTGTGTGTGT; R-TGGTGAGAGGACTGAGGAAGA)

560   OAS3 (F-GAAAACTGTCAAGGGAGGCTC; OAS3 R-CCCTCTGGTCCACATAGCTC)

561   HRV-01A (F- CAGGCCAAATTAAAGTCAATAAGC; R- AGGCTGAAGTTTGGTTTTGC)

562

563   ***Quantification and statistical analysis, RT-qPCR data***

564   GraphPad Prism (version 9.0.0) was used for data analysis. Data are shown as mean +/- S.E.M.

565   Statistical significance of differences between conditions was determined by t tests (two-tailed). Linear

566   regression analysis was used to determine association between clinical parameters, such as viral load

567   and NP CXCL10 in clinical samples and to test the null hypothesis that the slope of the association was

568   significantly different from zero. Non-linear regression analysis was used to fit viral growth to an

569   exponential curve (exponential growth with log(population)) to determine virus doubling times and to test

570   the null hypothesis that one curve fit both data sets for SARS-CoV-2 growth curve with and without

571   rhinovirus pre-infection. p<0.05 was considered statistically significant.

572

573   ***ELISA***

574   CXCL10 levels in cell-free residual nasopharyngeal swab samples or tissue culture supernatants was

575   quantified using a solid phase sandwich enzyme linked immunosorbent assay (ELISA) (Cat no: DY266,

576   R&D systems, MN). Briefly, frozen viral transport medium from residual nasopharyngeal swab samples

577   or basolateral medium from organoid cultures was thawed on ice and centrifuged to remove cell debris.

578   ELISA was performed according to the manufacturer's instructions.

579

580   **Single cell RNA-Seq of ALI organoid cultures**

581   *Library preparation and sequencing*

582   Organoid cultures were digested with trypsin/EDTA to form a single cell suspension. The 10X genomics

583   Single Cell 3' Protocol was used to produce Illumina-ready sequencing libraries with standard Illumina

584   paired-end constructs, according to the manufacturer's instructions.

585

586   *Analysis of scRNA-Seq data*

587   All downstream analyses were implemented using R version 3.6.3 and the package Seurat v3.1.4(Stuart

588   et al., 2019). The gene expression matrix mock and RV1A infected sample were first individually analyzed

589   in this procedure: Genes expressed in less than 3 cells and cells expressing less than 200 genes were

590   discarded. A distribution histogram of UMI count in all cells was made and cells with less than 8000 UMI

591   counts were discarded. This resulted in a matrix of 21086 genes expressing in 4511 cells in mock sample,

592   and a matrix of 21195 genes expressing in 4200 cells in RV1A infected sample. The raw counts were

593   normalized using the Seurat function NormalizeData with normalization.method = "LogNormalize" and

594   scale.facto = 10000. All genes are scaled using Seurat function ScaleData with default parameters.

25

595   Variable features were determined using method "vst". A total of top 2000 variable features were used

596   for principal component analysis (PCA). Graph based clustering was performed individually on mock and

597   RV1A infected sample. The KNN graph was built by FindNeighbors function with first 20 principal

598   components and k.param = 10. Louvain clustering was done using FindCluster function with resolution =

599   0.8 for both samples. Clusters were separately annotated in the mock and RV1A infected sample using

600   the following markers of the major cell groups in the airway epithelium: Basal Cycling (MKI67,

601   HIST1H4C), Basal (KRT14, KRT15, KRT5), Hillock (SPINK5, KRT13), Secretory (SCGB1A1, BPIFA1,

602   LYPD2), Ciliated (CAPS, PIFO, MORN2), Ionocyte (FOXI1) and PNEC(pulmonary neuroendocrine cells,

603   markers include AZGP1, AVIL)(Plasschaert et al., 2018). Each cluster found by clustering was assigned

604   to one of the above seven major groups. A group of developing ciliated cells with marker CCNO was

605   found in the mock sample and was merged into the ciliated cell cluster. After cluster annotation, mock

606   and infected samples were merged together to produce tSNE maps and make comparisons. Both

607   samples used same normalization method and the gene expression level was re-scaled. Dimensionality

608   reduction was performed by latent semantic analysis using Seurat function RunLSI with the first 50

609   singular values. The tSNE maps were then produced with the first 50 dimensions and perplexity 30. The

610   color coding of tSNE plots used cell type, sample source, viral read per cell and expression levels of

611   genes of interest.

612 **KEY RESOURCES TABLE**

REAGENT or RESOURCE	SOURCE	IDENTIFIER
Bacterial and Virus Strains		
HRV-01A	ATCC	ATCC VR-481
SARS-CoV-2	BEI resources	USA-WA1/2020
Biological Samples		
Residual nasopharyngeal samples from clinical testing	Yale-New Haven Hospital	
Chemicals, Peptides, and Recombinant Proteins		
BX795	Millipore Sigma	SML0694
Critical Commercial Assays		
iTaq Universal SYBR Green Supermix	BioRad	172-5125
iScript cDNA synthesis kit	BioRad	170-8891BUN
Primer-probe assay for SARS-CoV-2 (N1 gene)	IDT resources	10006600
Luna Universal Probe One-Step RT-qPCR Kit	New England Biolabs	E3006L
QIAamp Viral RNA isolation kit	QIAGEN	52904
QIAGEN RNeasy RNA isolation kit	QIAGEN	74106
Human CXCL10/IP-10 Duoset ELISA kit	R& D systems	DY266
Deposited Data		
Nasopharyngeal transcriptome data – deposited in GEO		
Single cell RNA-Seq data – deposited in GEO		
Experimental Models: Cell Lines		
NHBE-Bronchial Epi Cells for ALI	Lonza Walkersville Inc.	CC-2540S
H1 HeLa cells	ATCC	ATCC CRL-1958
Vero E6 cells	ATCC	ATCC CRL-1586
Oligonucleotides		
Primer sequences provided in Methods details		
Software and Algorithms		
R	www.r-project.org	SCR_001905
Seurat	satijalab.org/seurat/	RRID:SCR_016341
Prism v. 9.0.0 for MacOS	GraphPad	RRID:SCR_005375
Excel v. 16.43	Microsoft	RRID:SCR_016137
Ingenuity Pathway Analysis	QIAGEN	RRID: SCR_008653
Cytoscape	Open source	RRID: SCR_003032

613

614   References

615

616   Asgari, S., Schlapbach, L.J., Anchisi, S., Hammer, C., Bartha, I., Junier, T., Mottet-Osman, G., Posfay-

617   Barbe, K.M., Longchamp, D., Stocker, M*., et al.* (2017). Severe viral respiratory infections in children with

618   IFIH1 loss-of-function mutations. Proceedings of the National Academy of Sciences of the United States

619   of America *114*, 8342-8347.

620   Banerjee, A.K., Blanco, M.R., Bruce, E.A., Honson, D.D., Chen, L.M., Chow, A., Bhat, P., Ollikainen,

621   N., Quinodoz, S.A., Loney, C*., et al.* (2020). SARS-CoV-2 Disrupts Splicing, Translation, and Protein

622   Trafficking to Suppress Host Defenses. Cell.

623   Bastard, P., Rosen, L.B., Zhang, Q., Michailidis, E., Hoffmann, H.H., Zhang, Y., Dorgham, K.,

624   Philippot, Q., Rosain, J., Beziat, V*., et al.* (2020). Autoantibodies against type I IFNs in patients with life-

625   threatening COVID-19. Science *370*, eabd4585.

626   Blanco-Melo, D., Nilsson-Payant, B.E., Liu, W.C., Uhl, S., Hoagland, D., Moller, R., Jordan, T.X., Oishi,

627   K., Panis, M., Sachs, D*., et al.* (2020). Imbalanced Host Response to SARS-CoV-2 Drives Development

628   of COVID-19. Cell *181*, 1036-1045 e1039.

629   Byington, C.L., Ampofo, K., Stockmann, C., Adler, F.R., Herbener, A., Miller, T., Sheng, X., Blaschke,

630   A.J., Crisp, R., and Pavia, A.T. (2015). Community Surveillance of Respiratory Viruses Among Families

631   in the Utah Better Identification of Germs-Longitudinal Viral Epidemiology (BIG-LoVE) Study. Clinical

632   infectious diseases : an official publication of the Infectious Diseases Society of America *61*, 1217-1224.

633   Cevik, M., Tate, M., Lloyd, O., Maraolo, A.E., Scahfers, J., and A. Ho (2020). SARS-CoV-2, SARS-

634   CoV, and MERS-CoV viral load dynamics, duration of viral shedding, and infectiousness: a systematic

635   review and meta-analysis. The Lancet Microbe *20*, 30172-30175.

636   Clark, K., Plater, L., Peggie, M., and Cohen, P. (2009). Use of the pharmacological inhibitor BX795 to

637   study the regulation and physiological roles of TBK1 and IkappaB kinase epsilon: a distinct upstream

638   kinase mediates Ser-172 phosphorylation and activation. J Biol Chem *284*, 14136-14146.

639   Dong, E., Du, H, L Gardner (2020). An interactive web-based dashboard to track COVID-19 in real

640   time. ; published online Feb 19.

641   Essaidi-Laziosi, M., Geiser, J., Huang, S., Constant, S., Kaiser, L., and Tapparel, C. (2020). Interferon-

642   Dependent and Respiratory Virus-Specific Interference in Dual Infections of Airway Epithelia. Sci Rep

643   *10*, 10246.

644   Feld, J.J., et al (2020). Peginterferon-lambda for the treatment of COVID-19 in outpatients. MedRxiv,

645   https://doiorg/101101/2020110920228098.

646   Foxman, E.F., and Iwasaki, A. (2011). Genome-virome interactions: examining the role of common

647   viral infections in complex disease. Nature reviews Microbiology *9*, 254-264.

648   Foxman, E.F., Storer, J.A., Fitzgerald, M.E., Wasik, B.R., Hou, L., Zhao, H., Turner, P.E., Pyle, A.M.,

649   and Iwasaki, A. (2015). Temperature-dependent innate defense against the common cold virus limits

650   viral replication at warm temperature in mouse airway cells. Proceedings of the National Academy of

651   Sciences of the United States of America *112*, 827-832.

652   Galani, I.E., Rovina, N., Lampropoulou, V., Triantafyllia, V., Manioudaki, M., Pavlos, E., Koukaki, E.,

653   Fragkou, P.C., Panou, V., Rapti, V.*, et al.* (2021). Untuned antiviral immunity in COVID-19 revealed by

654   temporal type I/III interferon patterns and flu comparison. Nat Immunol *22*, 32-40.

655   Garcia-Sastre, A. (2017). Ten Strategies of Interferon Evasion by Viruses. Cell Host Microbe *22*, 176-

656   184.

657   Greer, R.M., McErlean, P., Arden, K.E., Faux, C.E., Nitsche, A., Lambert, S.B., Nissen, M.D., Sloots,

658   T.P., and Mackay, I.M. (2009). Do rhinoviruses reduce the probability of viral co-detection during acute

659   respiratory tract infections? J Clin Virol *45*, 10-15.

660   Hamano, E., Hijikata, M., Itoyama, S., Quy, T., Phi, N.C., Long, H.T., Ha, L.D., Ban, V.V., Matsushita,

661   I., Yanai, H.*, et al.* (2005). Polymorphisms of interferon-inducible genes OAS-1 and MxA associated with

662   SARS in the Vietnamese population. Biochem Biophys Res Commun *329*, 1234-1239.

663   He, J., Feng, D., de Vlas, S.J., Wang, H., Fontanet, A., Zhang, P., Plancoulaine, S., Tang, F., Zhan,

664   L., Yang, H*., et al.* (2006). Association of SARS susceptibility with single nucleic acid polymorphisms of

665   OAS1 and MxA genes: a case-control study. BMC Infect Dis *6*, 106.

666   He, X., Lau, E.H.Y., Wu, P., Deng, X., Wang, J., Hao, X., Lau, Y.C., Wong, J.Y., Guan, Y., Tan, X*., et*

667   *al.* (2020). Temporal dynamics in viral shedding and transmissibility of COVID-19. Nat Med *26*, 672-675.

668   Huang, J.T., Ran, R.X., Lv, Z.H., Feng, L.N., Ran, C.Y., Tong, Y.Q., Li, D., Su, H.W., Zhu, C.L., Qiu,

669   S.L*., et al.* (2020). Chronological Changes of Viral Shedding in Adult Inpatients With COVID-19 in Wuhan,

670   China. Clinical infectious diseases : an official publication of the Infectious Diseases Society of America

671   *71*, 2158-2166.

672   Isaacs, A., and Lindenmann, J. (1957). Virus interference. I. The interferon. Proc R Soc Lond B Biol

673   Sci *147*, 258-267.

674   Iwasaki, A. (2012). A virological view of innate immune recognition. Annu Rev Microbiol *66*, 177-196.

675   Janky, R., Verfaillie, A., Imrichova, H., Van de Sande, B., Standaert, L., Christiaens, V., Hulselmans,

676   G., Herten, K., Naval Sanchez, M., Potier, D*., et al.* (2014). iRegulon: from a gene list to a gene regulatory

677   network using large motif and track collections. PLoS Comput Biol *10*, e1003731.

678   Jartti, T., Jartti, L., Peltola, V., Waris, M., and Ruuskanen, O. (2008). Identification of respiratory

679   viruses in asymptomatic subjects: asymptomatic respiratory viral infections. Pediatr Infect Dis J *27*, 1103-

680   1107.

681   Karppinen, S., Toivonen, L., Schuez-Havupalo, L., Waris, M., and Peltola, V. (2016). Interference

682   between respiratory syncytial virus and rhinovirus in respiratory tract infections in children. Clin Microbiol

683   Infect *22*, 208 e201-208 e206.

684   Kim, D., Paggi, J.M., Park, C., Bennett, C., and Salzberg, S.L. (2019). Graph-based genome alignment

685   and genotyping with HISAT2 and HISAT-genotype. Nat Biotechnol *37*, 907-915.

686   Konno, Y., Kimura, I., Uriu, K., Fukushi, M., Irie, T., Koyanagi, Y., Sauter, D., Gifford, R.J., Consortium,

687   U.-C., Nakagawa, S*., et al.* (2020). SARS-CoV-2 ORF3b Is a Potent Interferon Antagonist Whose Activity

688   Is Increased by a Naturally Occurring Elongation Variant. Cell Rep *32*, 108185.

689   Kudo, E., Song, E., Yockey, L.J., Rakib, T., Wong, P.W., Homer, R.J., and Iwasaki, A. (2019). Low

690   ambient humidity impairs barrier function and innate resistance against influenza infection. Proceedings

691   of the National Academy of Sciences of the United States of America *116*, 10905-10910.

692   Lamborn, I.T., Jing, H., Zhang, Y., Drutman, S.B., Abbott, J.K., Munir, S., Bade, S., Murdock, H.M.,

693   Santos, C.P., Brock, L.G.*, et al.* (2017). Recurrent rhinovirus infections in a child with inherited MDA5

694   deficiency. J Exp Med *214*, 1949-1972.

695   Landry, M.L., and Foxman, E.F. (2018). Antiviral Response in the Nasopharynx Identifies Patients

696   With Respiratory Virus Infection. The Journal of infectious diseases *217*, 897-905.

697   Lee, J.S., and Shin, E.C. (2020). The type I interferon response in COVID-19: implications for

698   treatment. Nat Rev Immunol *20*, 585-586.

699   Liu, Y., Yan, L.M., Wan, L., Xiang, T.X., Le, A., Liu, J.M., Peiris, M., Poon, L.L.M., and Zhang, W.

700   (2020). Viral dynamics in mild and severe cases of COVID-19. Lancet Infect Dis *20*, 656-657.

701   Lokugamage, K.G., Hage, A., de Vries, M., Valero-Jimenez, A.M., Schindewolf, C., Dittmann, M.,

702   Rajsbaum, R., and Menachery, V.D. (2020). Type I Interferon Susceptibility Distinguishes SARS-CoV-2

703   from SARS-CoV. J Virol *94*, e01410-01420.

704   Love, M.I., Huber, W., and Anders, S. (2014). Moderated estimation of fold change and dispersion for

705   RNA-seq data with DESeq2. Genome Biol *15*, 550.

706   Lucas, C., Wong, P., Klein, J., Castro, T.B.R., Silva, J., Sundaram, M., Ellingson, M.K., Mao, T., Oh,

707   J.E., Israelow, B.*, et al.* (2020). Longitudinal analyses reveal immunological misfiring in severe COVID-

708   19. Nature *584*, 463-469.

709   Ma, X.Z., Bartczak, A., Zhang, J., He, W., Shalev, I., Smil, D., Chen, L., Phillips, J., Feld, J.J., Selzner,

710   N.*, et al.* (2014). Protein interferon-stimulated gene 15 conjugation delays but does not overcome

711   coronavirus proliferation in a model of fulminant hepatitis. J Virol *88*, 6195-6204.

712   Martin-Sancho, L., Lewinski, M.K., Pache, L., Stoneham, C.A., Yin, X., Pratt, D., Churas, C.,

713   Rosenthal, S.B., Liu, S., De Jesus, P.D.*, et al.* (2020). Functional Landscape of SARS-CoV-2 Cellular

714   Restriction. bioRxiv.

715   Mick, E., Kamm, J., Pisco, A.O., Ratnasiri, K., Babik, J.M., Castaneda, G., DeRisi, J.L., Detweiler,

716   A.M., Hao, S.L., Kangelaris, K.N.*, et al.* (2020). Upper airway gene expression reveals suppressed

717   immune responses to SARS-CoV-2 compared with other respiratory viruses. Nat Commun *11*, 5854.

718   Mihaylova, V.T., Kong, Y., Fedorova, O., Sharma, L., Dela Cruz, C.S., Pyle, A.M., Iwasaki, A., and

719   Foxman, E.F. (2018). Regional Differences in Airway Epithelial Cells Reveal Tradeoff between Defense

720   against Oxidative Stress and Defense against Rhinovirus. Cell Rep *24*, 3000-3007 e3003.

721   Monk, P.D., Marsden, R.J., Tear, V.J., Brookes, J., Batten, T.N., Mankowski, M., Gabbay, F.J., ,

722   Davies, D.E., Holgate, S.T., Ho, L., Clark, T., Djukanovic, R., Wilkinson, T.M.A. (2020). Safety and

723   efficacy of inhaled nebulised interferon beta-1a (SNG001) for treatment of SARS-CoV-2 infection: a

724   randomised, double-blind, placebo-controlled, phase 2 trial. Lancet Respiratory Medicine *20*, 30511-

725   30517.

726   Mulay, A., Konda, B., Garcia, G., Yao, C., Beil, S., Sen, C., Purkayastha, A., Kolls, J.K., Pociask, D.A.,

727   Pessina, P.*, et al.* (2020). SARS-CoV-2 infection of primary human lung epithelium for COVID-19

728   modeling and drug discovery. bioRxiv, https://wwwbiorxivorg/content/101101/20200629174623v1.

729   Nickbakhsh, S., Mair, C., Matthews, L., Reeve, R., Johnson, P.C.D., Thorburn, F., von Wissmann, B.,

730   Reynolds, A., McMenamin, J., Gunson, R.N.*, et al.* (2019). Virus-virus interactions impact the population

731   dynamics of influenza and the common cold. Proceedings of the National Academy of Sciences of the

732   United States of America.

733   Odendall, C., and Kagan, J.C. (2015). The unique regulation and functions of type III interferons in

734   antiviral immunity. Curr Opin Virol *12*, 47-52.

735   Olsen, S.J., Azziz-Baumgartner, E., Budd, A.P., Brammer, L., Sullivan, S., Pineda, R.F., Cohen, C.,

736   and Fry, A.M. (2020). Decreased Influenza Activity During the COVID-19 Pandemic - United States,

737   Australia, Chile, and South Africa, 2020. MMWR Morb Mortal Wkly Rep *69*, 1305-1309.

738   Onabajo, O.O., Banday, A.R., Stanifer, M.L., Yan, W., Obajemu, A., Santer, D.M., Florez-Vargas, O.,

739   Piontkivska, H., Vargas, J.M., Ring, T.J.*, et al.* (2020). Interferons and viruses induce a novel truncated

740   ACE2 isoform and not the full-length SARS-CoV-2 receptor. Nat Genet *52*, 1283-1293.

741   Pairo-Castineira, E., Clohisey, S., Klaric, L., Bretherick, A.D., Rawlik, K., Pasko, D., Walker, S.,

742   Parkinson, N., Fourman, M.H., Russell, C.D.*, et al.* (2020). Genetic mechanisms of critical illness in

743   Covid-19. Nature *https://www.nature.com/articles/s41586-020-03065-y*.

744   Pertea, M., Pertea, G.M., Antonescu, C.M., Chang, T.C., Mendell, J.T., and Salzberg, S.L. (2015).

745   StringTie enables improved reconstruction of a transcriptome from RNA-seq reads. Nat Biotechnol *33*,

746   290-295.

747   Pfaender, S., Mar, K.B., Michailidis, E., Kratzel, A., Boys, I.N., V'Kovski, P., Fan, W., Kelly, J.N., Hirt,

748   D., Ebert, N.*, et al.* (2020). LY6E impairs coronavirus fusion and confers immune control of viral disease.

749   Nat Microbiol *5*, 1330-1339.

750   Plasschaert, L.W., Zilionis, R., Choo-Wing, R., Savova, V., Knehr, J., Roma, G., Klein, A.M., and Jaffe,

751   A.B. (2018). A single-cell atlas of the airway epithelium reveals the CFTR-rich pulmonary ionocyte. Nature

752   *560*, 377-381.

753   Poole, S., Brendish, N.J., Tanner, A.R., and Clark, T.W. (2020). Physical distancing in schools for

754   SARS-CoV-2 and the resurgence of rhinovirus. Lancet Respir Med *8*, e92-e93.

755   Prevention, C.f.D.C.a. (2020). CDC 2019-Novel Coronavirus (2019-nCoV) Real-Time RT-PCR

756   Diagnostic Panel

757   Prevention, C.f.D.C.a. (2021). Emerging SARS-CoV-2 Variants.

758   Ravindra, N.G., Alfajaro, M.M., Gasque, V., Wei, J., Filler, R.B., Huston, N.C., Wan, H., Szigeti-Buck,

759   K., Wang, B., Montgomery, R.R.*, et al.* (2020). Single-cell longitudinal analysis of SARS-CoV-2 infection

760   in human bronchial epithelial cells. bioRxiv.

761   Rusinova, I., Forster, S., Yu, S., Kannan, A., Masse, M., Cumming, H., Chapman, R., and Hertzog,

762   P.J. (2013). Interferome v2.0: an updated database of annotated interferon-regulated genes. Nucleic

763   Acids Res *41*, D1040-1046.

764   Schneider, W.M., Chevillotte, M.D., and Rice, C.M. (2014). Interferon-stimulated genes: a complex

765   web of host defenses. Annual review of immunology *32*, 513-545.

766   Schultz-Cherry, S. (2015). Viral Interference: The Case of Influenza Viruses. The Journal of infectious

767   diseases *212*, 1690-1691.

768   Singanayagam, A., Patel, M., Charlett, A., Lopez Bernal, J., Saliba, V., Ellis, J., Ladhani, S., Zambon,

769   M., and Gopal, R. (2020). Duration of infectiousness and correlation with RT-PCR cycle threshold values

770   in cases of COVID-19, England, January to May 2020. Euro Surveill *25*.

771   Stuart, T., Butler, A., Hoffman, P., Hafemeister, C., Papalexi, E., Mauck, W.M., 3rd, Hao, Y., Stoeckius,

772   M., Smibert, P., and Satija, R. (2019). Comprehensive Integration of Single-Cell Data. Cell *177*, 1888-

773   1902 e1821.

774   Taylor, J.K., Coleman, C.M., Postel, S., Sisk, J.M., Bernbaum, J.G., Venkataraman, T., Sundberg,

775   E.J., and Frieman, M.B. (2015). Severe Acute Respiratory Syndrome Coronavirus ORF7a Inhibits Bone

776   Marrow Stromal Antigen 2 Virion Tethering through a Novel Mechanism of Glycosylation Interference. J

777   Virol *89*, 11820-11833.

778   Vanderheiden, A., Ralfs, P., Chirkova, T., Upadhyay, A.A., Zimmerman, M.G., Bedoya, S., Aoued, H.,

779   Tharp, G.M., Pellegrini, K.L., Manfredi, C.*, et al.* (2020). Type I and Type III Interferons Restrict SARS-

780   CoV-2 Infection of Human Airway Epithelial Cultures. J Virol *94*, e00985-00920.

781   Vogels, C.B.F., Brito, A.F., Wyllie, A.L., Fauver, J.R., Ott, I.M., Kalinich, C.C., Petrone, M.E.,

782   Casanovas-Massana, A., Catherine Muenker, M., Moore, A.J.*, et al.* (2020). Analytical sensitivity and

783   efficiency comparisons of SARS-CoV-2 RT-qPCR primer-probe sets. Nat Microbiol *5*, 1299-1305.

784   Wang, N., Zhan, Y., Zhu, L., Zheng, Z., Lu, Y., Hong, P. (2020). Retrospective Multicenter Cohort

785   Study Shows Early Interferon Therapy Is Associated with Favorable Clinical Responses in COVID-19

786   Patients. Cell Host Microbe *28*, 455-464.

787   Wolfel, R., Corman, V.M., Guggemos, W., Seilmaier, M., Zange, S., Muller, M.A., Niemeyer, D., Jones,

788   T.C., Vollmar, P., Rothe, C.*, et al.* (2020). Virological assessment of hospitalized patients with COVID-

789   2019. Nature *581*, 465-469.

790   Wolsk, H.M., Folsgaard, N.V., Birch, S., Brix, S., Hansel, T.T., Johnston, S.L., Kebadze, T., Chawes,

791   B.L., Bonnelykke, K., and Bisgaard, H. (2016). Picornavirus-Induced Airway Mucosa Immune Profile in

792   Asymptomatic Neonates. The Journal of infectious diseases *213*, 1262-1270.

793   Wu, A., Mihaylova, V.T., Landry, M.L., and Foxman, E.F. (2020). Interference between rhinovirus and

794   influenza A virus: a clinical data analysis and experimental infection study. Lancet Microbe *1*, e254-e262.

795   Xia, H., Cao, Z., Xie, X., Zhang, X., Chen, J.Y., Wang, H., Menachery, V.D., Rajsbaum, R., and Shi,

796   P.Y. (2020). Evasion of Type I Interferon by SARS-CoV-2. Cell Rep *33*, 108234.

797   Yahya, M., Rulli, M., Toivonen, L., Waris, M., and Peltola, V. (2017). Detection of Host Response to

798   Viral Respiratory Infection by Measurement of Messenger RNA for MxA, TRIM21, and Viperin in Nasal

799   Swabs. The Journal of infectious diseases *216*, 1099-1103.

800   Yilmaz, A., Marklund, E., Andersson, M., Nilsson, S., Andersson, L.M., Lindh, M., and Gisslen, M.

801   (2020). Upper respiratory tract levels of SARS-CoV-2 RNA and duration of viral RNA shedding do not

802   differ between patients with mild and severe/critical COVID-19. The Journal of infectious diseases *223*,

803   15-18.

804   Yu, J., Peterson, D.R., Baran, A.M., Bhattacharya, S., Wylie, T.N., Falsey, A.R., Mariani, T.J., and

805   Storch, G.A. (2019). Host Gene Expression in Nose and Blood for the Diagnosis of Viral Respiratory

806   Infection. The Journal of infectious diseases *219*, 1151-1161.

807   Zhang, Q., Bastard, P., Liu, Z., Le Pen, J., Moncada-Velez, M., Chen, J., Ogishi, M., Sabli, I.K.D.,

808   Hodeib, S., Korol, C.*, et al.* (2020). Inborn errors of type I IFN immunity in patients with life-threatening

809   COVID-19. Science *370*, eabd4570.

810   Zheng, S., Fan, J., Yu, F., Feng, B., Lou, B., Zou, Q., Xie, G., Lin, S., Wang, R., Yang, X.*, et al.* (2020).

811   Viral load dynamics and disease severity in patients infected with SARS-CoV-2 in Zhejiang province,

812   China, January-March 2020: retrospective cohort study. BMJ *369*, m1443.

813   Zhou, Z., Ren, L., Zhang, L., Zhong, J., Xiao, Y., Jia, Z., Guo, L., Yang, J., Wang, C., Jiang, S.*, et al.*

814   (2020). Heightened Innate Immune Responses in the Respiratory Tract of COVID-19 Patients. Cell Host

815   Microbe *27*, 883-890 e882.

816   Ziegler, C.G.K., Allon, S.J., Nyquist, S.K., Mbano, I.M., Miao, V.N., Tzouanas, C.N., Cao, Y., Yousif,

817   A.S., Bals, J., Hauser, B.M.*, et al.* (2020). SARS-CoV-2 Receptor ACE2 Is an Interferon-Stimulated Gene

818   in Human Airway Epithelial Cells and Is Detected in Specific Cell Subsets across Tissues. Cell *181*, 1016-

819   1035 e1019.

820   Zou, L., Ruan, F., Huang, M., Liang, L., Huang, H., Hong, Z., Yu, J., Kang, M., Song, Y., Xia, J.*, et al.*

821   (2020). SARS-CoV-2 Viral Load in Upper Respiratory Specimens of Infected Patients. N Engl J Med *382*,

822   1177-1179.

823

Figures

Fig 1. Transcriptome analysis of RNA isolated from SARS-CoV-2+ nasopharyngeal swabs

Fig 2. Relationship between nasopharyngeal (NP) CXCL10 and viral load in 140 SARS-CoV-2+ patients.

Fig 3. Viral load and nasopharyngeal CXCL10 patterns in vivo over time

Fig 4. Kinetics of SARS-CoV-2 replication in organoids and in vivo.

Fig 5. Effect of prior rhinovirus infection on ISG induction and SARS-CoV-2 replication in human airway epithelial organoids.

Fig 6. Effect of blocking ISG induction on SARS-CoV-2 replication following rhinovirus infection.

Fig 7. Effect of blocking ISG induction on SARS-CoV-2 replication in a low MOI infection
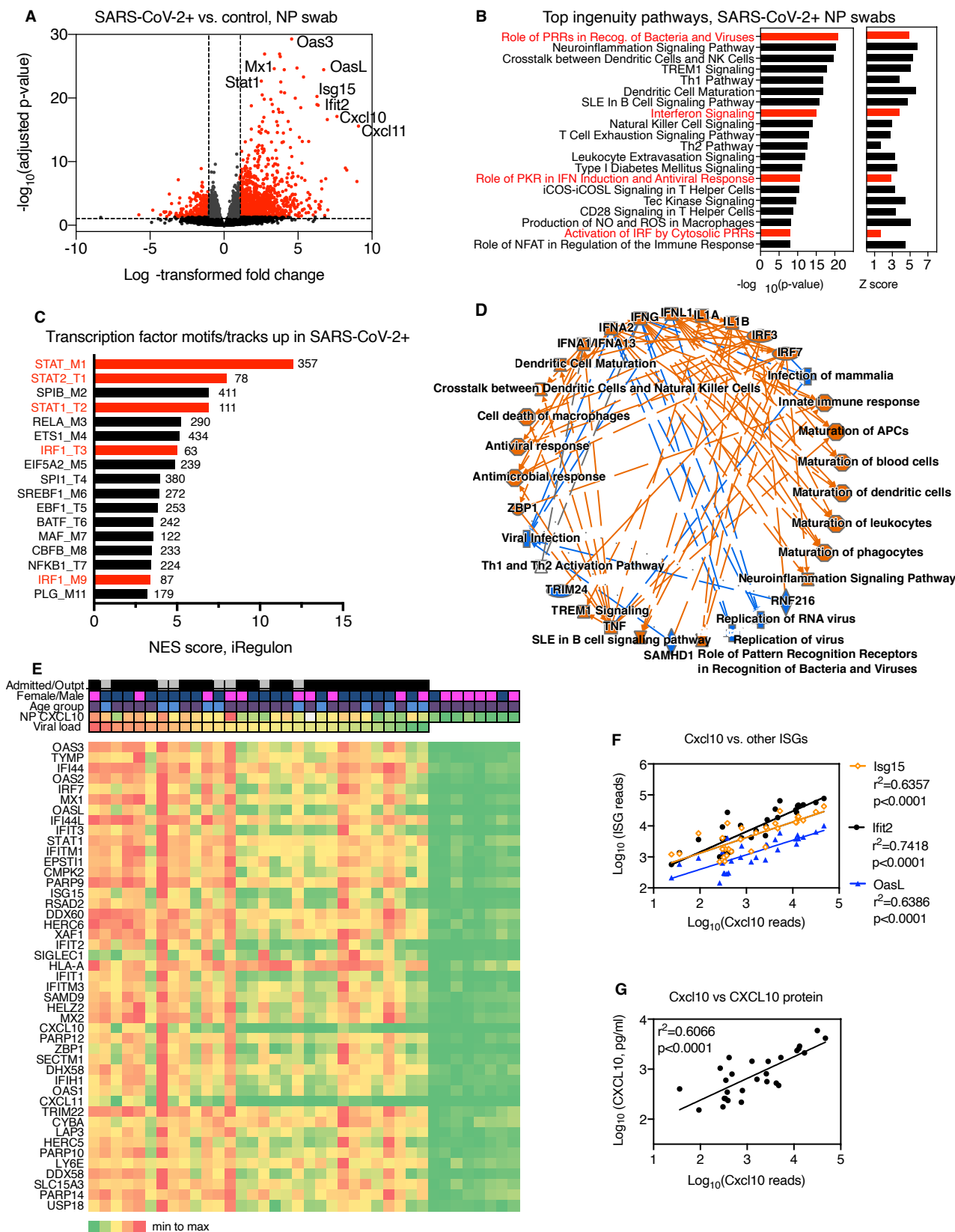
Fig 1. Transcriptome analysis of RNA isolated from SARS-CoV-2+ nasopharyngeal swabs.

Fig 1. Transcriptome analysis of RNA isolated from SARS-CoV-2+ nasopharyngeal swabs (related to Fig S1).

(A) Volcano plot showing significantly differentially expressed protein-coding genes based on RNASeq of NP swab RNA from SARS-CoV-2 patients (n=30) compared to control SARS-CoV-2 negative subjects (n=8). Transcripts with fold change>2, adjusted p-value<0.05 are highlighted in red.

(B) Top 20 ingenuity pathways enriched in SARS-CoV-2+ compared to controls, based on 1770 differentially expressed RNAs. P-value and Z-score for each pathway is indicated on the x-axis. Pathways related to interferon and interferon regulatory factor (IRF) signaling are highlighted in red.

(C) Transcription factor binding sites associated with NP transcripts enriched in SARS-CoV-2+ patients compared to controls. Bars show strength of association of motifs/tracks with enriched transcripts, indicated by NES score. Y-axis label indicates top transcription factor associated with each cluster of motifs (M) or tracks (T) and the cluster code. Number of enriched transcripts associated with each track/motif is indicated to the right of each bar. Transcription factors associated with the interferon response are highlighted in red.

(D) Graphical summary of pathways and regulators enriched based on ingenuity pathway analysis of differentially expressed genes enriched in NP RNA of SARS-CoV-2+ patients compared to controls.

(E) Heatmap showing relative expression level of top 45 most significant differentially expressed genes in patients (left) or SARS-CoV-2-negative controls (right). Clinical characteristics of each patient are indicated by color: viral load (red=highest viral load/lowest Ct value, green=lowest viral load/highest Ct value); NP CXCL10 protein level (red=highest, green=lowest, white=data not available). Heatmap colors represent values from highest (red) to lowest (green) for viral load (based on Ct value), CXCL10 concentration (pg/ml), or gene expression level, scaled from minimum to maximum (green=0; yellow=0.5, red=1) Patient characteristics indicated at the top of the graph include Admission status (grey=outpatient, black= admitted); Gender (blue=male, pink=female); Age (blue<55yrs, purple>60 yrs.) White = data not available.

(F) Correlation between reads mapping to CXCL10 and reads mapping to other ISGs (Ifit2, OasL, Isg15).

(G) Correlation between reads mapping to Cxcl10 and CXCL10 protein measured by ELISA in NP swab-associated viral transport medium.
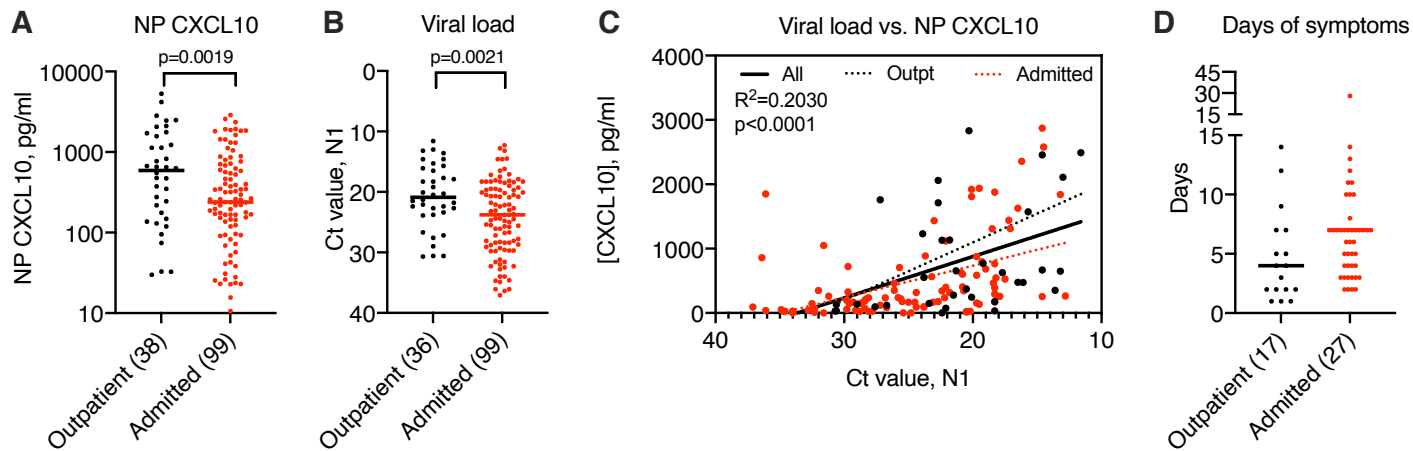
Fig 2 (related to Fig S2). Relationship between nasopharyngeal (NP) CXCL10 and viral load in 140 SARS-CoV-2+ patients.

(A) NP CXCL10 level in patients testing positive for SARS-CoV-2 by RT-qPCR at Yale-New Haven Hospital in March 2020. Black symbols indicate patients tested as outpatients or in the emergency department and not admitted to the hospital, red symbols indicate patients admitted to the hospital.

(B) Ct value for SARS-CoV-2 N1 gene in outpatients and admitted patients. Number in parenthesis (A, B) indicates number of outpatient (total n=38) and admitted (total n=102) samples for which data was available.

(C) Regression analysis showing relationship between viral load and NP CXCL10 protein for all samples (black solid line, r^2 and p-value indicated) or for only outpatients (dashed black line) or admitted patients (dotted red line).

(D) Days of symptoms reported prior to testing for samples with this information available (number indicated n parentheses).
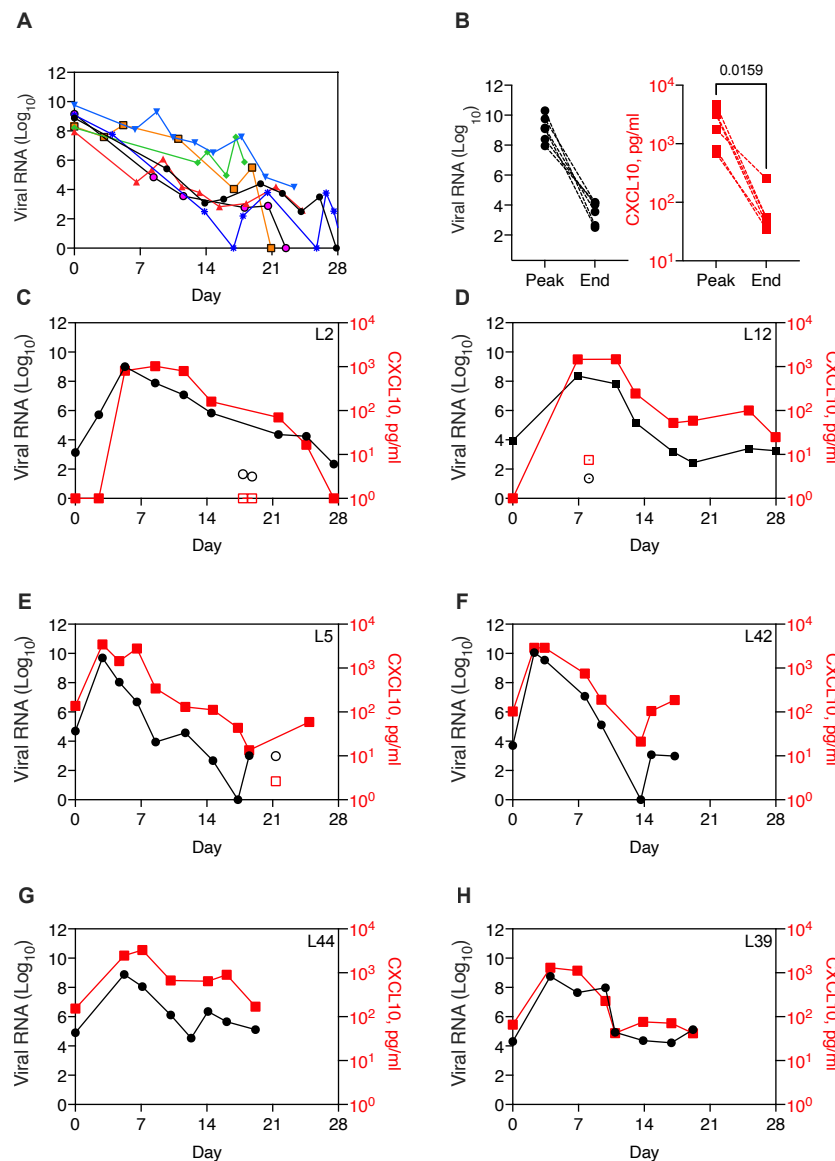
Fig 3 (related to Table S1). Nasopharyngeal viral load and CXCL10 in patients diagnosed prior to peak viral load.

(A) Viral load over time in seven longitudinal samples from patients with high viral load in first sample (Ct N1>20).

(B) Paired viral RNA and NP CXCL10 measurements at the peak viral load and at the end viral load, defined as the first sample with Ct N1>30, for 6 patients shown in (G) (data not available for one sample). CXCL10 level was significantly different in peak and end samples by paired t-test.

(C) – (H) Viral load and NP CXCL10 level in longitudinal samples from SARS-CoV-2+ patients who presented with a low viral load (Ct N1>28) that increased to a high viral load (Ct N1<20). Viral load is expressed as fold change from the limit of detection for the SARS-CoV-2 N1 gene (black circles) and CXCL10 is expressed as pg/ml in the NP-swab associated viral transport medium (red squares).   Samples with low levels of RnaseP, an indicator of sample quality, are shown with open symbols. Patient characteristics are described in Table S5.
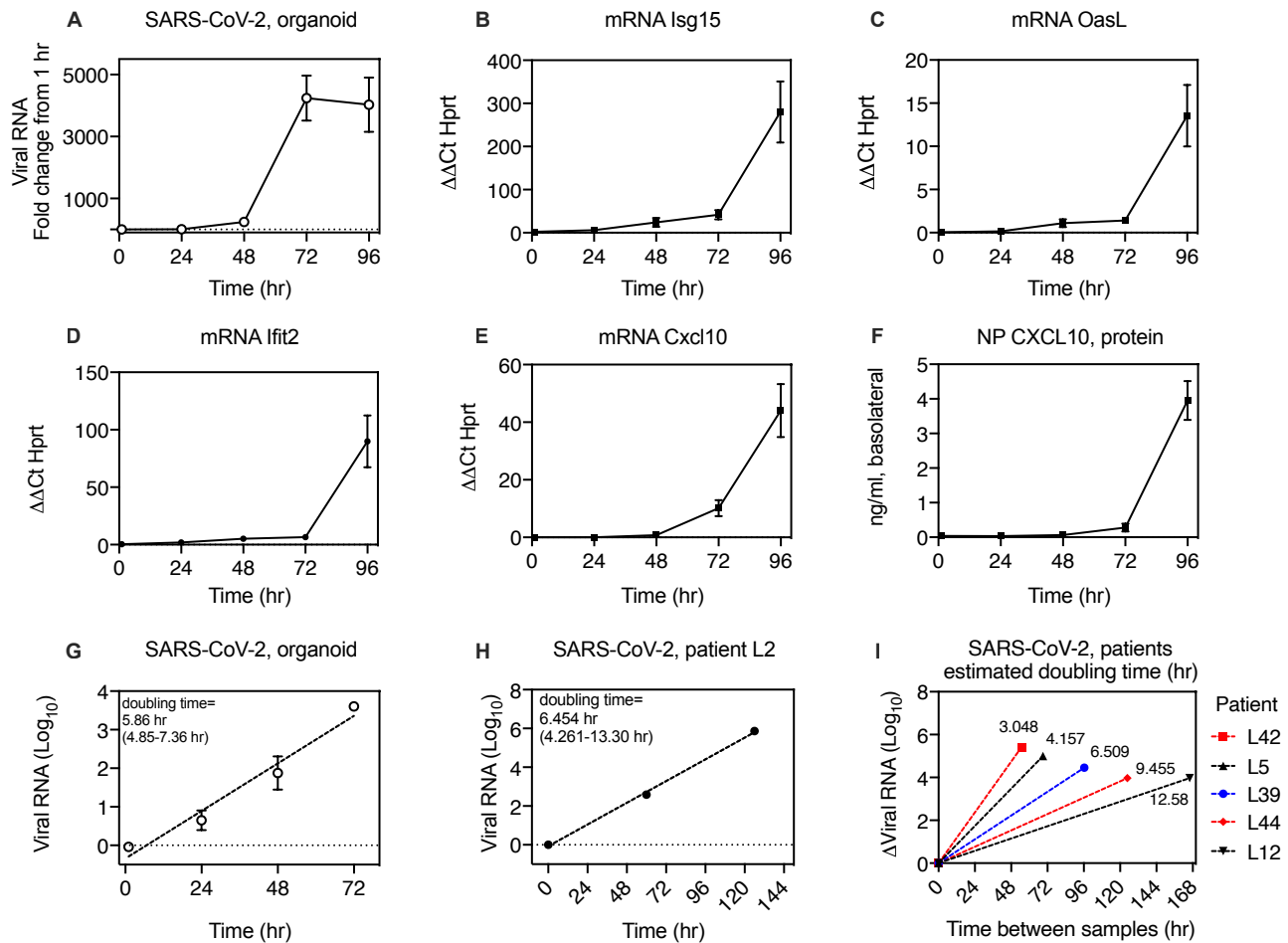
Figure 4. Kinetics of SARS-CoV-2 replication in organoids and in vivo.
(A) Time course of SARS-CoV-2 replication in human primary airway epithelial organoids, expressed as fold increase from 1hr (post-inoculation time point).
(B) - (E) ISG mRNA level relative to HPRT mRNA in organoids during SARS-CoV-2 infection.
(F) CXCL10 protein in the basolateral medium during SARS-COV-2 replication. For A-H, symbols show mean and S.E.M. of five biological replicates per condition.
(G) Exponential curve fit for increase in RNA during SARS-CoV-2 during replication in organoids from 1-72 hr and calculated doubling time for exponential growth.
(H) Exponential curve fit for increase in viral RNA during SARS-CoV-2 replication for first three virus-positive samples from patient L2 and calculated doubling time for exponential growth with 95% confidence interval.
(I) Estimated doubling times for increase in viral RNA during SARS-CoV-2 replication in patients with one SARS-CoV-2 positive sample prior to peak viral load, shown in fig 3 B-F. Y-axis shows change in viral RNA and x-axis shows time interval between samples. Doubling time calculation assumes exponential growth between first and peak viral load samples.
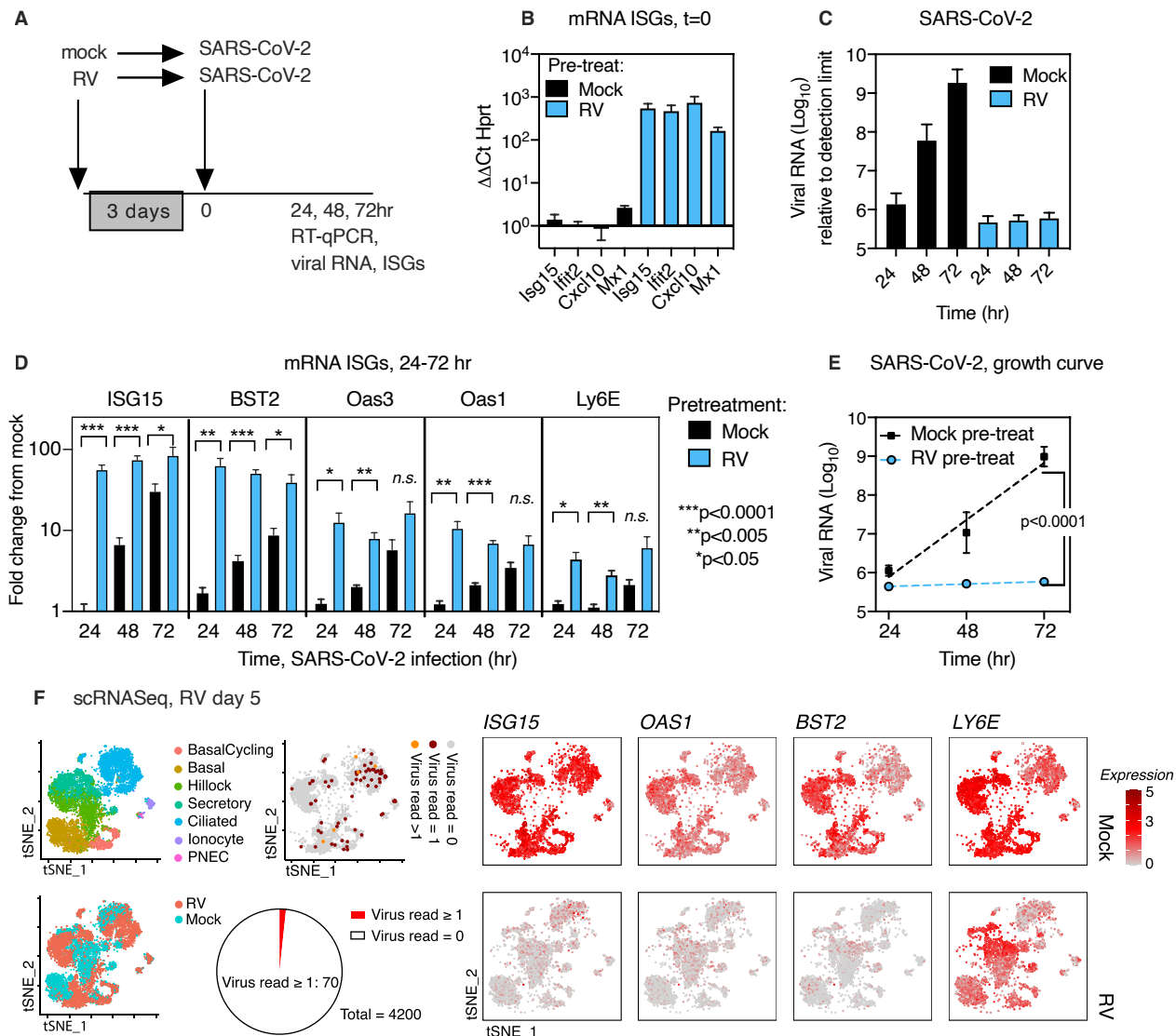
Figure 5. Effect of prior rhinovirus infection on ISG induction and SARS-CoV-2 replication in human airway epithelial organoids.

(A) Timing of infection of epithelial organoids with rhinovirus followed by SARS-CoV-2

(B) Expression of interferon stimulated genes in airway epithelial organoids 3 days post-rhinovirus infection, relative to mRNA for the housekeeping gene HPRT

(C) SARS-CoV-2 viral RNA at 24, 48, and 72 hr post-infection, with or without RV pre-infection

(D) Expression of interferon stimulated genes at 24, 48, and 72 hr post SARS-CoV-2 infection, with or without RV pre-infection, expressed as fold change from uninfected cells

(E) Replication of SARS-CoV-2 in mock- vs. rhinovirus-pretreated cultures, fit to exponential growth curve

(F) Single cell sequencing of human airway epithelial cell organoids, mock or 5 days post rhinovirus infection. Red and orange dots indicate 70/4200 cells with detectable viral RNA at this time point in rhinovirus-infected cultures (at least 1 read from viral RNA).   TSNE plots show expression of mRNA for ISGs in mock and infected cultures at the same time point.
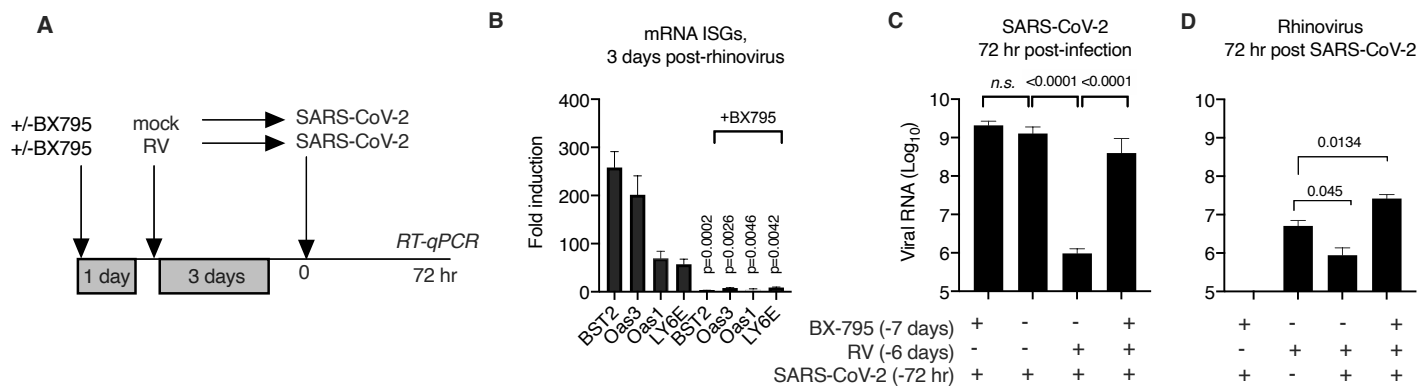
Figure 6. Effect of pretreatment with BX795 during sequential rhinovirus, SARS-CoV-2 infection

Organoid cultures were pretreated with or without BX795 for 18 hr, then mock-infected or infected with HRV01A, incubated for 3 days, then infected with SARS-CoV-2.

(A) Effect of BX-795 pre-treatment on ISG induction, 3 days post rhinovirus infection. Bars show fold change in ISG mRNA level in RV infected cultures compared to mock without (left) or with (right) BX-795 pre-treatment. P values indicate significant differences between ISG levels in cultures with or without BX795 pretreatment by t-test.

(B) SARS-CoV-2 viral RNA level relative to the limit of detection in organoid cultures, 72 hr post SARS-CoV-2 infection, with and without BX-795 and/or RV pre-treatment. P values indicate significant differences in viral RNA levels, n.s. = not significant.

(C) HRV01A viral RNA level relative to the limit of detection in organoid cultures, 72 hr post SARS-CoV-2 infection, with and without BX-795 and/or RV pre-treatment. This graph also includes cultures infected with RV but not subsequently infected with SARS-CoV-2. P values indicate significant differences in viral RNA levels.

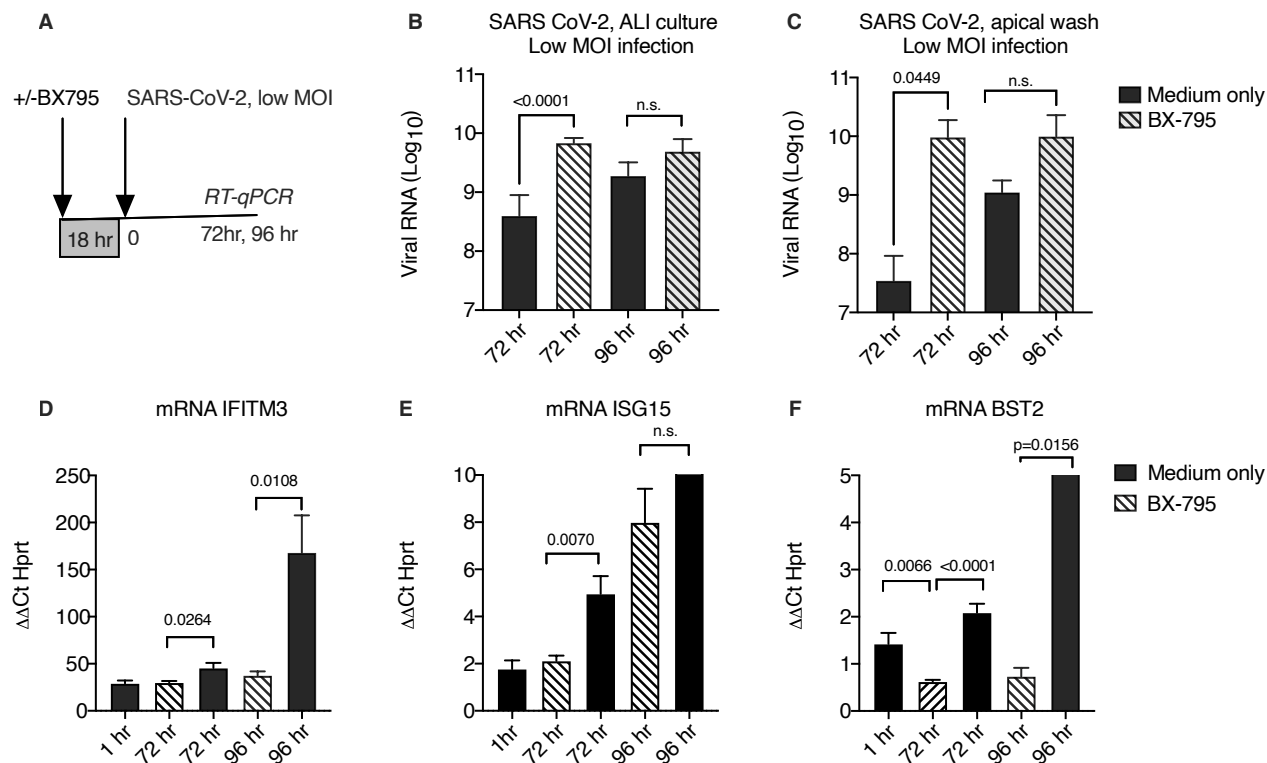For all graphs, bars show mean and S.E.M. of 4-6 biological replicates per condition.

Fig 7. Effect of BX795 on SARS-CoV-2 replication in low MOI infection

(A) Cultures were pre-treated with 6μM BX-795 or medium only, then inoculated with SARS-CoV-2, MOI 0.05, at t=0 hr. Cultures were collected for RNA isolation and RT-qPCR at t=1, 72, and 96 hr post infection. Apical wash was collected at 72 and 92 hr post-infection.

(B)SARS-CoV-2 viral RNA in RNA isolated from organoid cultures 72 hr and 96 hr post-inoculation, with (hatched bars) or without BX795 (black bars), relative to the limit of detection.

(C)SARS-CoV-2 viral RNA in RNA isolated from the apical wash of cultures collected at 72 hr and 96 hr post-inoculation, with (hatched bars) or without BX795 (black bars), relative to the limit of detection.

(D)-(F) ISG mRNA level in SARS-CoV-2 infected cultures, graphed relative to the mRNA level for the housekeeping gene HPRT ($2^{Ct\text{-}Ct\ HPRT}$), at 1, 72, or 96 hr post-inoculation.

(B)-(F) Bars show mean and S.E.M. for 4-6 biological replicates per condition. P-values are shown for significant differences, based on the students t-test.